Effect of Concrete Strength on Axial Load Response of Circular Columns

by

Pedro Da Silva

March 2000

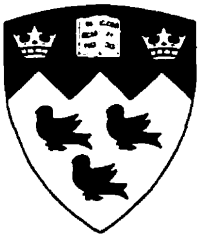

Department of Civil Engineering and Applied Mechanics

McGill University

Montréal, Canada

A thesis submitted to the Faculty of Graduate Studies
and Research in partial fulfilment of the requirements
for the degree of Master of Engineering

Effect of Concrete Strength on Axial Load Response of Circular Columns

Abstract

The behaviour of 10 spirally reinforced concrete columns and 5 plain concrete columns subjected to a concentric compressive load is investigated. The reinforced concrete columns were designed using the CSA A23.3-94 Standard. The experimental specimens were made of concretes with compressive strengths ranging from 35 MPa to 125 MPa. Two types of steel spiral reinforcement, Grade 400 and Grade 500, were used to investigate the ability of a higher yield strength steel to confine the concrete core.

The response of the reinforced specimens is compared to predictions using a stress-strain model for confined concrete. The determination of the predicted response is based on the computation of a load-strain response using the effective confining stresses in the concrete core. The effects of the concrete compressive strength and the steel spiral tensile strength on the load-strain response are investigated. The peak loads of the spirally reinforced circular concrete columns are compared to the peak loads predicted by our current codes of practice.

The response of the plain concrete columns with a wide range of specified compressive strengths are investigated. The peak loads of the plain concrete columns are predicted using various concrete stress-block factors provided by different codes.

Les effets de la résistance en compression du béton sur le comportement axial des poteaux circulaires

Résumé

Ce rapport présente une étude expérimentale sur le comportement en compression de 10 poteaux circulaires en béton armé et 5 poteaux non armés. Les poteaux en béton armé ont été conçus selon la norm CSA A.23.3-94. Les spécimens expérimentaux ont été construits avec du béton d'une résistance spécifiée en compression variant de 35 MPa à 125 MPa. Deux types d'armature, nuance 400 et nuance 500, ont été utilisés pour étudier les effets de l'utilisation d'acier d'armature à haute résistance pour confiner le noyau central du béton.

Le comportement des spécimens armés est comparé à un modèle contrainte-déformation de béton confiné. La prédiction du comportement est basée sur la contrainte effective du noyau central du béton. Les effets de la résistance en compression du béton et la résistance en tension de l'armature sur le comportement contrainte-déformation sont analysés. Les charges ultimes des poteaux armés sont comparées aux charges ultimes indiquées dans nos codes de pratique courante.

Le comportement des poteaux non armés selon différentes résistances spécifiées en compression est aussi etudié. Les charges ultimes des poteaux non armés sont prédites à l'aide des modèle de distribution de contraintes normal utilisès dans divers normes.

Acknowledgements

I would like to express my deepest gratitude to Professor Denis Mitchell and Dr. William Cook for their guidance, encouragement and valuable advice throughout this research program. The assistance of Patrick Paultre of Université de Sherbrooke is also appreciated.

The research program was carried out in the Structures Laboratory at McGill University. The author wishes to thank Ron Sheppard, Marek Przykorski, John Bartczak and Damon Kiperchuk for their assistance in the laboratory. The author would also like to thank, Stuart Bristowe, Pierre Koch, Bryce Tupper, Emmet Poon, Kevin Li, Carla Ghannoum and Wassim Ghannoum for their assistance throughout the program.

The completion of this project would not have been possible without the effort and assistance of the secretaries of the Civil Engineering Department, particularly Sandy Shewchuk-Boyd, Lilly Nardini, Ann Bless, and Donna Sears.

The donation of materials by Lafarge Canada for this research project was also greatly appreciated.

Finally, the author would like to thank his friends and family, for their support, patience and encouragement during his years at McGill.

Pedro Da Silva
March, 2000

Table of Contents

List of Figures

Chapter 1

Chapter 2

Chapter 3

Chapter 4

List of Tables

List of Symbols

A_c	=	area of core of spirally reinforced compression member measured to outside diameter of spiral;
A_g	=	gross cross-sectional area of section;
A_p	=	area of prestressing tendon;
A_{shx}	=	total cross-sectional area of the transverse reinforcement perpendicular to the x-axis;
A_{shy}	=	total cross-sectional area of the transverse reinforcement perpendicular to the y-axis;
A_{sp}	=	cross-sectional area of the spiral reinforcement;
A_{st}	=	total area of longitudinal reinforcement;
A_t	=	area of structural steel shape, pipe, or tubing in a composite section;
$A_{\varepsilon 0}$	=	area under the load-strain curve integrated from ε =0 until $\varepsilon = \varepsilon_{C50C}$;
c_x	=	side dimension of concrete core parallel to x-axis;
c_y	=	side dimension of concrete core parallel to y-axis :
d_b	=	longitudinal bar diameter;
d_c	=	outside diameter of the spiral reinforcement;
d_s	=	diameter of spiral;
E_c	=	modulus of elasticity of concrete;
f'_c	=	specified compressive strength of concrete;
f_{co}	=	maximum compressive strength of a plain concrete member;
f_{cc}	=	maximum compressive strength of confined concrete;
f_{hcc}	=	stress in the transverse reinforcement at the maximum strength of confined concrete;
f_l	=	lateral confining pressure applied on the concrete core from transverse reinforcement;
f_{le}	=	effective lateral confining stress applied on the concrete core.
f_{pr}	=	stress in prestressing tendons when concrete reaches limiting compressive strain;
f_{sp}	=	tensile yield stress the spiral reinforcement;
f_y	=	specified yield strength of reinforcement;
F_y	=	specified yield strength of structural steel section;
f_{yh}	=	specified yield strength of transverse reinforcement;
k_e	=	confinement effectiveness coefficient;
k	=	coefficient affecting slope of the ascending branch on the stress-strain curve;
k_1	=	coefficient affecting slope of the descending branch on the stress-strain curve;
k_2	=	coefficient affecting curvature of the descending branch on the stress-strain curve;
N^*	=	design axial load at ultimate limit state;
P_{max}	=	maximum design axial load carried by test specimen
P_{ro}	=	factored axial load resistance at zero eccentricity;
p_t	=	ratio of non-prestressed longitudinal column reinforcement = A_{st}/A_g;
s	=	centre to centre spacing of the spiral;
s'	=	clear spacing between the ties;
α_1	=	ratio of average stress in rectangular compression block to specified concrete strength;
ε_{cc}	=	maximum strain at at f_{cc} under confinement;
ε_{co}	=	strain at f'_c;
ε_{hcc}	=	strain in transverse reinforcement steel correponding to f_{hcc};
ε_{C50C}	=	axial strain in confined concrete when stress drops to $0.5f_{cc}$;
ε_y	=	yield strain of reinforcement steel.
ϕ	=	strength reduction factor;
ρ_h	=	volumetric ratio of transverse reinforcement in the concrete core;
ρ_s	=	volumetric ratio of longitudinal reinforcement in the column cross-section.

Chapter 1

Introduction

1.1 Overview

In recent years High-Strength Concrete (HSC) has increasingly gained acceptance in the construction industry. This acceptance has occurred so quickly that it has been difficult for codes of practice to keep pace with the changes. Research in this field is therefore required to update and to validate our present codes of practice.

HSC offer significant benefits such as an increase in compressive strength, and an increase in durability. An increase in compressive strength will lead to a reduction in member size and an economy of materials, while an increase in durability will lead to a lower life-cycle cost. However, HSC does not behave in the same manner as normal-strength concrete. As the concrete's compressive strength increases, so does its brittleness. The ductility of high-strength concrete is only a fraction of that of normal-strength concrete. Low ductility in concrete is detrimental to its performance in areas of high seismic activity. Therefore, HSC members should be designed differently than normal-strength concrete members.

Concrete columns require lateral steel reinforcement to improve ductility. As the concrete compressive strength is increased in a column, the regular Grade 400 steel reinforcement may not be strong enough to adequately confine a column' s concrete core without requiring extremely small spacings of confinement reinforcement.

This paper will study and check the validity of the current codes of practice used in the design of high-strength circular columns and check whether the use of high-strength confinement steel is a valid solution to increase the column's ductility. The compressive

stress-strain response of the reinforced concrete columns will be modeled using procedures developed in the literature.

1.2 Code Requirements for Confinement of Circular Columns

1.2.1 CSA A23.3-94 and ACI 318-89

The basic design equation for a circular column's reinforcement is given by:
(Clause 10.9.4. in the CSA Standard (CSA, 1994) and Clause 10.9.3 in the ACI Code (ACI, 1989))

$$\rho_s = 0.45\left(\frac{A_g}{A_c} - 1\right)\frac{f_c'}{f_{yh}} \qquad (1.1)$$

where, (as given in CSA A23.3-94)

A_c = area of core of spirally reinforced compression member measured to outside diameter of spiral,

A_g = gross area of section,

f'_c = specified compressive strength of concrete,

f_{yh} = specified yield strength of transverse reinforcement,

ρ_s = ratio of volume of spiral reinforcement to total volume of core (out-to-out of spirals), of a spirally reinforced compression member.

In regions with high seismic activity an additional design equation must be satisfied. CSA Clause 21.4.4.2 (ACI Clause 21.4.4.1) requires that the volumetric ratio, ρ_s, not be less than the following equation:

$$\rho_s = 0.12 \frac{f_c'}{f_{yh}} \tag{1.2}$$

This additional requirement is to ensure that large columns have sufficient confinement and ductility. Equation 1.1 is not conservative enough for large columns due to the reduced A_g/A_c ratio. As the column's diameter is increased, the A_g/A_c ratio becomes smaller. Equation 1.2 is therefore applicable for large columns in which the A_g/A_c ratio is less than 1.27.

Equation 1.1 is not an empirical equation. It was derived analytically, based on certain assumptions made by ACI Committee 105 in 1933. It has been used in the ACI Code ever since. This equation is based on an approach that equates the loss associated with the spalling of the concrete cover, to the strength enhancement provided by the reinforcement spiral. The following assumptions were used. First, the strength of shell concrete was taken as 0.75 f'_c, nine-tenths that of the core concrete which was assumed to be 0.85 f'_c. Secondly, the compressive strength of the confined concrete was assumed to increase by 15 percent. (ACI,1933). This gives the following expression,

$$2\rho_s f_{yh} A_c = 1.15x0.75 f_c' (A_g - A_c) \tag{1.3}$$

Solving for the required volumetric ratio, ρ_s, Eq.1.3 becomes Eq.1.1.

The specifications for spirals are given in Clause 7.6.4 (CSA, 1994). This clause states that the spiral reinforcement be at least 6 mm in diameter, that the pitch be less than one-sixth the core diameter and that the clear spacing between successive turns of a spiral not exceed 75 mm nor be less than 25 mm.

1.2.2 The New Zealand Standard: NZS 3101

In the New Zealand Standard (NZS, 1995) the basic equation for the design of a circular concrete column's spiral reinforcement is to be taken as the larger of Eq.1.4 or Eq.1.5, (Clause 8.4.7.1) as given by:

$$\rho_s = \frac{(1 - p_t m)}{2.4} \frac{A_g}{A_c} \frac{f'_c}{f_{yh}} \frac{N^*}{\phi f'_c A_g} - 0.0084 \qquad (1.4)$$

where, A_g/A_c shall not be taken less than 1.2 and $p_t m$ shall not be taken greater than 0.4.

$$\rho_s = \frac{A_{sl}}{155 d_c} \frac{f_y}{f_{yh}} \frac{1}{d_b} \qquad (1.5)$$

In Eq.1.4 and Eq.1.5, f_{yh} must not be taken larger than 800 MPa.

In seismic regions (potential plastic hinge regions), the ratio of spiral reinforcement is to be taken as the larger of Eq.1.6 or Eq.1.7. (Clause 8.5.4.3) given by:

$$\rho_s = \frac{(1.3 - p_t m)}{2.4} \frac{A_g}{A_c} \frac{f'_c}{f_{yh}} \frac{N^*}{\phi f'_c A_g} - 0.0084 \qquad (1.6)$$

where, A_g/A_c shall not be taken less than 1.2 and $p_t m$ shall not be taken greater than 0.4

$$\rho_s = \frac{A_{sl}}{110 d_c} \frac{f_y}{f_{yh}} \frac{1}{d_b} \qquad (1.7)$$

where.

A_c	=	area of concrete core of section measured to outside of peripheral spiral or hoop,
A_g	=	gross area of section,
A_{st}	=	total area of longitudinal reinforcement.
d_b	=	longitudinal bar diameter,
d_c	=	diameter of concrete core of circular column measured to outside spiral or circular hoop,
f'_c	=	specified compressive strength of concrete,
f_y	=	lower characteristic yield strength of non-prestressed reinforcement,
f_{yh}	=	lower characteristic yield strength of spiral. hoop, stirrup-tie or supplementary cross-tie reinforcement.
m	=	$f_y/(0.85 f'_c)$.
N^*	=	design axial load at ultimate limit state.
p_t	=	ratio of non-prestressed longitudinal column reinforcement = A_{st}/A_g.
ϕ	=	strength reduction factor.
ρ_s	=	ratio of volume of spiral or hoop reinforcement to total volume of concrete core (out-to-out of spirals or hoops).

1.3 Code Equations for Ultimate Strength of Concrete Columns

1.3.1 Canadian Standard: CSA A23.3-94

Clause 10.10.4 of the Canadian Standard Association Standard A23.3 (CSA, 1994) requires that the factored axial load resistance of a reinforced concrete column be limited to P_{rmax}, where:

$P_{max} = 0.85\ P_{ro}$ for spirally reinforced columns (1.8)

$P_{max} = 0.80\ P_{ro}$ for tied columns (1.9)

The pure factored axial load capacity, P_{ro}, is given by:

$$P_{ro} = \alpha_1 \phi_c f_c' \left(A_g - A_{st} - A_t - A_p\right) + \phi_s f_y A_{st} + \phi_a F_y A_t - f_{pr} A_p \tag{1.10}$$

Where the stress block factor, α_1, is:

$$\alpha_1 = 0.85 - 0.0015 f_c' \geq 0.67 \tag{1.11}$$

The terms in these expressions are defined as:

A_g = gross area of section,

A_p = area of prestressing tendon,

A_{st} = total area of longitudinal steel,

A_t = area of structural steel shape, pipe, or tubing in a composite section,

f_c' = specified concrete strength of concrete,

f_{pr} = stress in prestressing tendons when concrete reaches limiting compressive strain,

f_y = specified yield strength of reinforcement,

F_y = specified yield strength of structural steel section,

P_{ro} = factored axial load resistance at zero eccentricity,

α_1 = ratio of average stress in rectangular compression block to specified concrete strength,

ϕ_a = resistant factor for structural steel, taken as 0.9,

ϕ_c = resistant factor for concrete, taken as 0.6,

ϕ_s = resistant factor for reinforcement bars, taken as 0.85.

1.3.2 American Concrete Institute Code: ACI 318-89

Clause 10.3.5 of the American Concrete Institute Code (ACI, 1989) requires that the factored axial load resistance of a reinforced concrete column be limited to $P_{n(max)}$, where:

$$\phi P_{n(\max)} = 0.85\phi\left[0.85 f_c'\left(A_g - A_{st}\right) + f_y A_{st}\right] \quad \text{for spiral columns} \tag{1.12}$$

$$\phi P_{n(\max)} = 0.80\phi\left[0.85 f_c'\left(A_g - A_{st}\right) + f_y A_{st}\right] \quad \text{for tied columns} \tag{1.13}$$

The terms in these expressions are defined in the ACI code as:

A_g = gross area of section,

A_{st} = total area of longitudinal reinforcement,

f'_c = specified compressive strength of concrete,

f_y = specified yield strength of non-prestressed reinforcement,

ϕ = strength reduction factor, taken as 0.75.

1.3.3 New Zealand Standard: NZS 3101

Clause 8.5.1.3 of the New Zealand Standard (NZS. 1995) requires that the design axial load in compression at ultimate limit state, N*, shall not exceed, $0.85\phi N_o$. The nominal compressive strength of a concrete column is given by:

$$N_o = \alpha_1 f_c' \left(A_g - A_{st}\right) + \phi_s f_y A_{st} \tag{1.14}$$

Where the stress block factor α_1, is:

$$\alpha_1 = 0.85 \qquad \text{for } f_c' \leq 55 \text{ MPa} \tag{1.15a}$$

$$\alpha_1 = 0.85 - 0.004\left(f_c' - 55\right) \geq 0.75 \qquad \text{for } f_c' > 55 \text{ MPa} \tag{1.15b}$$

The terms in these expressions are defined by the NZS 3101 as:

A_g = gross area of section.

A_{st} = total area of longitudinal reinforcement.

f_c' = specified compressive strength of concrete.

f_y = specified yield strength of non-prestressed reinforcement.

N_o = critical load given by Eq.1.14.

N^* = design axial load at ultimate limit state.

α_1 = factor defined by Eq.1.15.

ϕ_s = strength reduction factor.

The NZS has an additional requirement for design in seismic regions. The design axial load in compression at ultimate limit state, N^* , shall not exceed, $0.7\phi N_o$.

1.3.4 Comparison of the Three Codes

Both the CSA Standard and ACI Code follow the same approach in finding the ultimate strength of a column, except for the value of the stress block factor, α_1. The ACI Code assumes that stress block factor,α_1, is constant for the full range of concrete strengths. while the CSA Standard assumes that α_1 will decrease linearly as the concrete's compressive strength is increased. The New Zealand Standard's philosophy is somewhere between that of the CSA Standard and that of the ACI Code. The NZS assumes that α_1 is constant at 0.85 up to 55 MPa and then decreases linearly with concrete compressive strengths above 55 MPa. Figure 1.1 compares the variation of the stress block factor, α_1 for the ACI Code, CSA Standard and NZS Standard as a function of specified concrete strength.

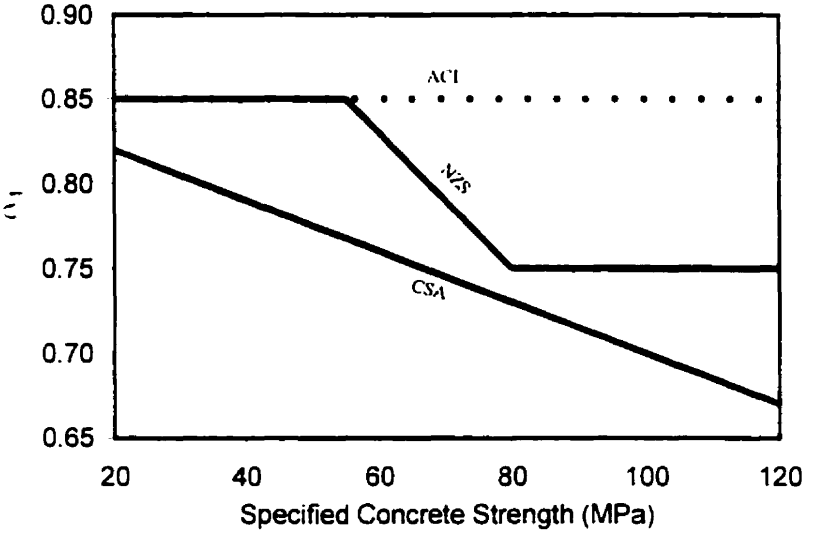

Figure 1.1:Comparison of α_1 factors of various codes

1.4 Previous Research on Confinement of High-Strength Concrete

The strength enhancement of confined concrete has been known and studied for many years. Considère (1903) was the first to introduce spiral reinforcement as confinement in concrete in 1899. It was not until 1928, that the effect of the confined concrete was fully investigated in the famous University of Illinois experiments by Richart, Brandtzaeg and Brown (1928). In 1928 Richart, *et al.* reported on tests on the effects of confined normal-strength concrete using a lateral fluid pressure with varying intensities. From these tests, Richart *et al.* developed the following equations for the influence of confinement on the confined strength, f_{cc} and the associated peak strain ϵ_{cc}:

$$f_{cc} = f_c' + k_1 f_l \tag{1.16}$$

$$\varepsilon_{cc} = \varepsilon_{co}\left(1 + k_2 \frac{f_l}{f_c'}\right) \tag{1.17}$$

where,

f_{cc} = maximum concrete stress due to confinement,

f'_c = specified concrete strength,

f_l = lateral confining stress,

k_1 = confinement factor, taken as 4.1

k_2 = confinement factor, taken as $5k_1$

ε_{cc} = maximum strain at at f_{cc} under confinement,

ε_{co} = strain at f'_c.

In subsequent experiments, Richart *et al.* (1929) discovered that the increase in the concrete's compressive strength due to closely spaced steel spirals was approximately the same as the increase in compressive strength due to lateral fluid pressure. The concrete confinement stress produced by the spirals, f_l, is calculated on the assumption that the steel

spiral has yielded and hence equating the tensile yield strength force (2 A_{sp} f_{yh}) with the compressive confining pressure on the core (f_l d_c s) gives the following expression:

$$f_l = \frac{2A_{sp}f_{yh}}{d_c s} \tag{1.18}$$

where,

A_{sp} = cross-sectional area of the spiral reinforcement,

d_c = outside diameter of the spiral reinforcement,

f_{yh} = tensile yield stress the spiral reinforcement,

s = centre-to-centre spacing of the spiral.

In 1978, Iyengar *et al.* (1978) improved Richart's equation by adding a correction factor (1-s/d_c) and by increasing k_1 from 4.1 to 4.6. Confinement becomes less effective as the spiral's pitch is increased. In Eq.1.19, Iyengar *et al.* took this into account. The confinement in Eq.1.19 is reduced as the reinforcement's pitch approached the column diameter, resulting in a confined concrete strength given as:

$$f'_{cc} = f'_c + 4.6 f_l (1 - s/d_c) \tag{1.19}$$

The first research performed on the confinement of high-strength concrete was by Ahmad and Shah (1982). Concrete with strengths as high as 69 MPa were tested. It was found that as the concrete's compressive strength was increased, the effectiveness of the lateral confinement decreased.

Martinez, Nilson, and Slate (1984) tested 94 short confined columns (diameters of 4, 5, and 6 inches) with concrete strength varying from 21 to 69 MPa. They found that the concrete's compressive strength and strain at maximum stress all increased with an increase

in confinement stress, regardless the concrete strength. The modulus of elasticity of confined concrete was found to be approximately the same as that of unconfined concrete. The authors also postulated that the use of very high strength spirals may be somewhat unconservative because the assumption that the spiral steel yields, may not be true. The expressions developed by Martinez, Nilson and Slate for confined concrete are given as:

$$f_{cc} = f_c' + 4.0 f_l \left(1 - s/d_c\right) \quad \text{for normal-weight concrete} \tag{1.20}$$

$$f_{cc} = f_c' + 1.8 f_l \left(1 - s/d_c\right) \quad \text{for light-weight concrete} \tag{1.21}$$

Pessiki and Pieroni, (1997) studied the axial load behaviour of large (22 inch diameter) spirally reinforced high-strength concrete columns. The columns were made of concrete with strengths varying from 34.5 MPa to 69 MPa. They discovered that ACI Code's Clause 10.3.5.1 can be used to accurately predict a column's strength from 34.5 MPa to 52.7 MPa. Above this strength, it was found that Clause 10.3.5.1 over-predicts the column's strength. It was found that an increase in the size and pitch of a spiral, while maintaining a constant volume of spiral reinforcement led to a decrease in the specimen's ductility, confirming the validity of effective confinement. The ductility of the columns was found to decreased as the specified concrete strength, f'_c, increased.

Zahn, Park, and Priestley (1987) investigated the use of a higher grade steel for transverse confining spiral reinforcement in columns with a diameter of 400 mm. Six normal-strength (20.5 MPa to 27.3 MPa) reinforced concrete columns, with either Grade 380 steel or Grade 275 steel, were subjected to uniform monotonic compression load. It was found that the volumetric ratio of the confining reinforcement can be decreased with increasing steel yield strength without resulting in a reduction in compressive strength of the confined concrete, and that the ductility of the confined concrete, although reduced, remained high. It was also observed that the ultimate longitudinal compressive strain, that is when first fracture of a steel spiral occurs, is decreased as a higher grade of steel spiral is used.

Mander, Priestley and Park (1988) observed the stress-strain behaviour of confined concrete. Twelve full-size specimens, 500 mm in diameter and 1500 mm in height, were tested. Both Grade 275 and Grade 380 spirals were used. Normal-Strength concrete having a specified compressive strength of 28 MPa was used. It was observed that the fracture strain of the high-strength steel is about 40% lower than that of the medium-strength steel.

1.5 Previous Research on the Stress-Strain Response of Confined Concrete

Mander, Priestley and Park (1988) developed a unified stress-strain approach that is valid for both circular and rectangular columns. The stress-strain model is based on the research of Popvics (1973). The concrete compressive stress, f_c, can be expressed as:

$$f_c = \frac{f_{cc} x r}{r - 1 + x^r} \tag{1.22}$$

where:

f_{cc} = compressive strength of confined concrete,

r = $E_c/(E_c - E_{sec})$,

E_c = $5000\,(f'_c)^{0.5}$ MPa is the tangent of the elasticity of the concrete,

E_{sec} = f_{cc}/ε_{cc},

f'_c = compressive strength of unconfined concrete,

x = $\varepsilon_c / \varepsilon_{cc}$.

The confinement stresses in the concrete are not constant between the ties or spirals. Mander *et al.* (1988) assumed that there was arching action between the confining ties or spirals. The arching action was assumed to be parabolic with an initial slope of 45° (See Fig.1.2). From this assumption, k_e, the confinement effectiveness coefficient was developed

to represent an average confinement stress acting on the concrete core. The following equations give the confinement effectiveness coefficients for circular hoops, circular spirals, and rectangular hoops respectively:

$$k_e = \frac{\left(1 - \frac{s'}{2d_s}\right)^2}{1 - \rho_g} \qquad \text{(for circular hoops)} \qquad (1.23)$$

$$k_e = \frac{1 - \frac{s'}{2d_s}}{1 - \rho_g} \qquad \text{(for circular spirals)} \qquad (1.24)$$

$$k_e = \frac{\left(1 - \frac{\sum w_i^2}{6b_c d_c}\right)\left(1 - \frac{s'}{2b_c}\right)\left(1 - \frac{s'}{2d_c}\right)}{\left(1 - \rho_g\right)} \qquad \text{(for rectangular hoops)} \qquad (1.25)$$

where,

b_c = concrete core dimension to centre line of perimeter hoop in x-direction.

d_c = concrete core dimension to centre line of perimeter hoop in y-direction.

d_s = diameter of spiral.

s' = clear spacing between the ties.

Σw_i^2 = sum of the squares of all the clear spacing between adjacent longitudinal steel bars in rectangular section.

ρ_g = longitudinal reinforcement ratio in the core section.

The effective confinement pressure, f_{le} is given as:

$$f_{le} = k_e f_l \qquad (1.26)$$

where:

f_l = lateral confining pressure applied on the concrete core from transverse reinforcement,

f_{le} = effective lateral confining stress applied on the concrete core,

k_e = confinement effectiveness coefficient.

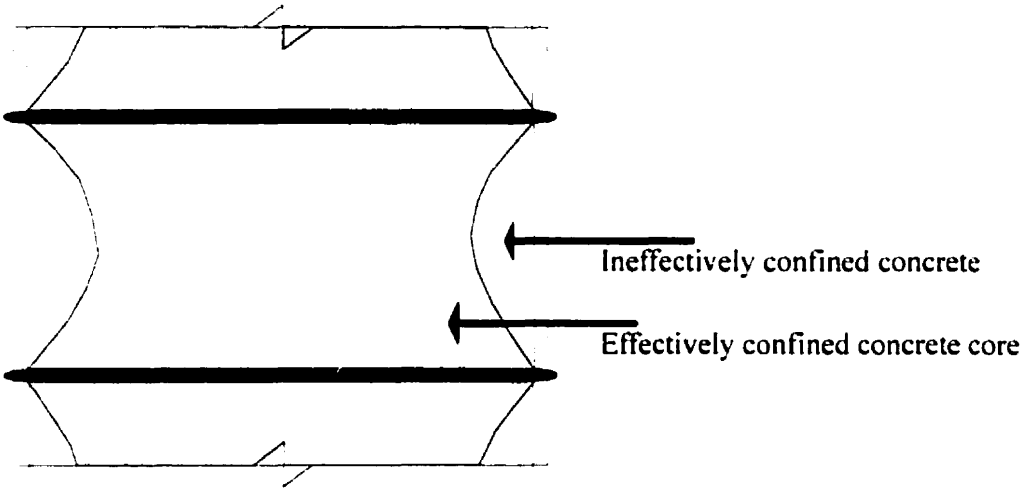

Figure 1.2: Arching Action in Confined Concrete

The general confinement model used by Mander, Priestley and Park (1988) was one that was developed by William and Warnke (1975) and is given by:

$$f_{cc} = f_{co}\left(-1.254 + 2.254\sqrt{1 + \frac{7.94 f_{le}}{f_{co}}} - 2\frac{f_{le}}{f_{co}}\right) \qquad (1.28)$$

Cusson and Paultre (1995) proposed a stress-strain model for the response of high-strength concrete square columns. The maximum strength of the confined concrete, f_{cc}, was given as:

$$f_{cc} = f_{co} + 4.1 f_{le} \tag{1.29}$$

where.

f_{co} = maximum strength of unconfined concrete in a member. taken as 0.85 f'_c.

f_l = nominal lateral pressure applied on the concrete core.

The nominal lateral pressure on tied rectangular columns was taken as:

$$f_l = \frac{f_{hcc}}{s}\left(\frac{A_{shx} + A_{shy}}{c_x + c_y}\right) \tag{1.30}$$

where.

A_{shx} = total cross-sectional area of the transverse reinforcement perpendicular to the x-axis.

A_{shy} = total cross-sectional area of the transverse reinforcement perpendicular to the y-axis.

c_x = side dimension of concrete core parallel to x-axis.

c_y = side dimension of concrete core parallel to y-axis.

f_{hcc} = stress in the transverse reinforcement at the maximum strength of confined concrete.

s = centre-to centre tie spacing.

The confinement of tied concrete columns is assumed not to be uniform throughout the column. Like Mander *et al.*(1988). Cusson and Paultre (1995) assumed an arching action to act in the form of a parabola with an initial tangent slope of 45°. A confinement effectiveness coefficient was therefore used to take the arching action into account. The effective confinement coefficient. k_e. represents the ratio of the smallest effectively confined concrete area. midway between the ties. to the nominal concrete core. A_c. Cusson used k_e. derived by Mander and given in Eq.1.25.

The effective confinement pressure, k_e, for rectangular columns is therefore given by:

$$f_{le} = k_e f_l = k_e \frac{f_{lcc}}{s}\left(\frac{A_{shx} + A_{shy}}{c_x + c_y}\right) \tag{1.31}$$

Cusson and Paultre (1995) proposed a stress-strain response based on the work by Mander *et al.* (1988). This stress-strain response is broken into two parts, the ascending branch and the descending branch. The ascending branch is modeled using the relationship derived by Popovic (1973) (See Eq.1.22). Equation 1.22, requires ε_{cc}, the longitudinal compression strain corresponding to f_{cc}. Using experimental data, Cusson and Paultre developed an expression for ε_{cc}, which is given as:

$$\varepsilon_{cc} = \varepsilon_{co} + 0.21\left(\frac{f_{le}}{f_{co}}\right)^{1.7} \tag{1.32}$$

The descending branch was based on a stress-strain relation developed by Fatitis and Shah (1985) is given as:

$$f_c = f_{cc} \cdot \exp\left[k_1 (\varepsilon_c - \varepsilon_{cc})^{k_2}\right] \tag{1.33}$$

where,

k_1 = coefficient affecting slope of the descending branch of the stress-strain curve.

$$k_1 = \frac{\ln 0.5}{(\varepsilon_{f\,50c} - \varepsilon_{cc})^{k_2}} \tag{1.33a}$$

k_2 = coefficient affecting curvature of the descending branch of the stress-strain curve.

$$k_2 = 0.58 + 16\left(f_{le}/f_{co}\right)^{1.4} \tag{1.33b}$$

ε_{C50C} = axial strain in condined concrete when stress drops to $0.5f_{cc}$.

$$\varepsilon_{c50c} = 0.004 + 0.15\left(f_{le}/f_{co}\right)^{1.1} \tag{1.33c}$$

Cusson and Paultre (1995) also developed an iterative procedure to compute the stress in the lateral ties for rectangular columns, f_{hcc}. The iterative procedure can compute the confining stress by using the following expression:

$$\varepsilon_{hcc} = 0.5\varepsilon_{cc} - \left[1 - \left(\frac{f_{le}}{f_{cc}}\right)\right] \tag{1.34}$$

where,

f_{cc} = maximum compressive strength of the confined concrete member.

f_{le} = effective confinement pressure in the concrete core.

f_{hcc} = stress in transverse reinforcement at maximum strength of confined concrete.

ε_{cc} = axial strain in the concrete corresponding to f_{cc}.

ε_{hcc} = strain in transverse reinforcement steel correponding to f_{hcc}.

The steps in this iterative procedure are as follows:

1. Compute the effective confinement pressure, f_{le}, with stress $f_{hcc} = f_{hy}$ in the transverse reinforcement.
2. Estimate the peak strength of the confined concrete, f_{cc}, and the corresponding strain, ε_{cc}.
3. Estimate the ε_{hcc} in the transverse reinforcement with Eq.1.34.
4. Find the resulting stress f_{hcc} in the transverse steel using the stress-strain relationship of the steel confinement reinforcement.

5. Re-evaluate the effective confinement pressure, f_{le}, with the new value of f_{hcc}, only if $f_{hcc} < f_{yh}$.
6. Repeat step 2 to 5 until the value f_{le} converges.

1.6 Objectives of this Experimental Research

The objective of this research program is to investigate a number of issues related to confinement of high-strength concrete columns. An experimental program was planned to investigate the following parameters:

1) The reduction of concrete ductility as the concrete compressive strength is increased:
2) The effectiveness of a higher grade steel in confining the concrete core: and
3) To determine accuracy of current stress-strain confined concrete models.

A comparison between predictions using current codes of practice and the experimental results will also be performed. The purpose is to evaluate the different approaches and determine which design philosophy is more appropriate for the design of high-strength concrete columns.

Chapter 2

Experimental Program

2.1 Design and Details of Column Specimens

Fifteen concrete circular columns were constructed and tested in the Jamieson Structures Laboratory in the Department of Civil Engineering and Applied Mechanics at McGill University. Each of these specimens were tested under a compressive concentric load using a 11 400 kN MTS universal testing machine.

All fifteen columns are identical in size, 1600 mm in height and 305 mm (12 inches) in diameter with a 15 mm cover. The fifteen columns were cast in five series of three, each series with a different concrete strength. The nominal concrete strengths were 30 MPa, 40 MPa, 60 MPa, 100 MPa, and 120 MPa, thus encompassing a wide spectrum of concrete strengths. Figure 2.1 shows the dimensions of the test specimens.

Each of the five test series consisted of three columns. The first column in each series was reinforced with Grade 400, hot-rolled, deformed steel spiral reinforcement. The second column in each series was reinforced with Grade 500 cold-rolled deformed steel spiral reinforcement. And thirdly, a plain column was constructed with no longitudinal or transverse steel. The diameters of the Grade 400 and Grade 500 spiral reinforcing bars were 11.3 mm and 9.5 mm, respectively. The amount longitudinal steel was kept constant in the twelve reinforced concrete columns. Six No. 20 (d_b = 19.5 mm , A_s = 300 mm^2) bars were used in each column. The longitudinal reinforcement ratio of each reinforced column, ρ_g, was 2.46%, thus satisfying the minimum requirement of at least one percent of longitudinal reinforcement.

The spirals in each reinforced concrete column were anchored by bending the free ends of the spirals, at the top and bottom of the column, into the column core. The free end anchorage length were at least $15d_b$ as shown in Fig. 2.1. This end anchorage detail was provided so that the spirals would remain functional after spalling of the concrete cover.

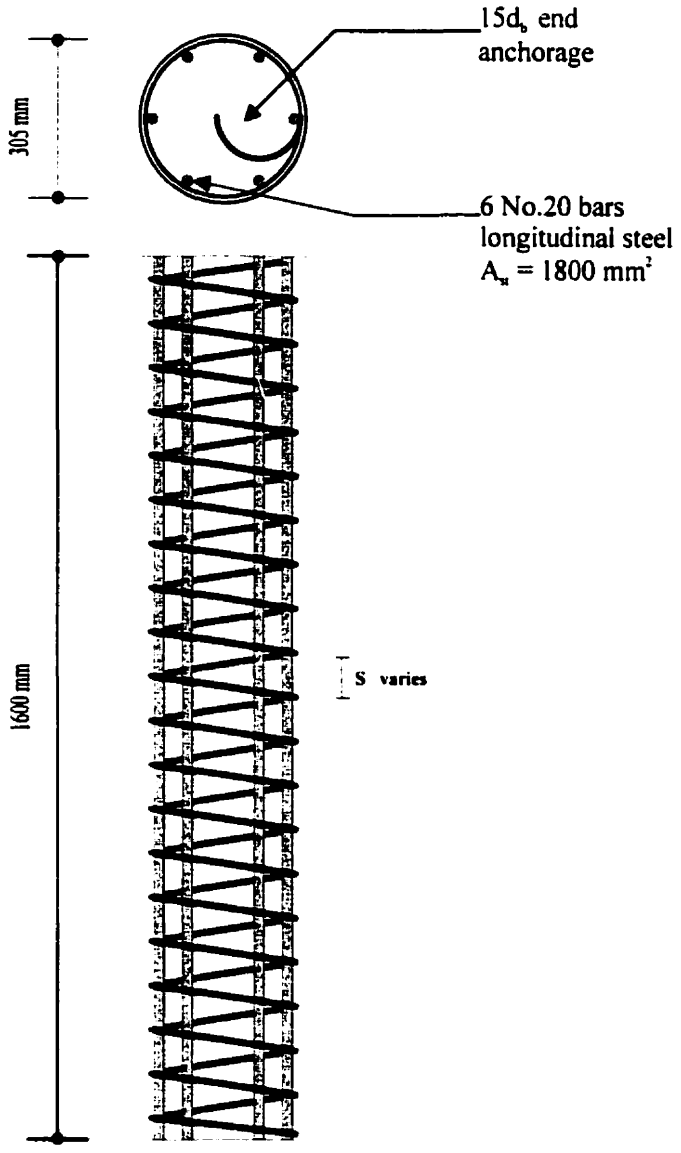

Figure: 2.1 Dimensions of a Typical Test Column

The specimens in this experimental program were named in the following manner, C#-#. The letter C is used to identify the specimens as columns, the first number following the letter C identifies the nominal concrete compressive strength while the second number identifies the grade of spiral reinforcement. For instance C40-400 would identify the column as having a target concrete strength of 40 MPa and a Grade 400 steel spiral reinforcement. Table 2.1 lists the properties of the individual specimens.

Table 2.1: Test specimen details

Specimen	Longitudinal Reinforcement			Spiral Reinforcement				Concrete
	Amount	f_y (MPa)	ρ_g (%)	d_b (mm)	s (mm)	ρ_s (%)	f_{yh} (MPa)	f'_c (MPa)
C30-0	--	--	--	--	--	--	--	35.5
C30-400	6 No. 20	407	2.46	11.3	100	1.40	440	35.5
C30-500	6 No. 20	407	2.46	9.5	100	1.00	560	35.5
C40-0	--	--	--	--	--	--	--	39.5
C40-400	6 No. 20	407	2.46	11.3	100	1.40	440	39.5
C40-500	6 No. 20	407	2.46	9.5	100	1.00	560	39.5
C60-0	--	--	--	--	--	--	--	59.6
C60-400	6 No. 20	407	2.46	11.3	75	1.86	440	59.6
C60-500	6 No. 20	407	2.46	9.5	80	1.24	560	59.6
C100-0	--	--	--	--	--	--	--	119.9
C100-400	6 No. 20	407	2.46	11.3	45	3.11	440	119.9
C100-500	6 No. 20	407	2.46	9.5	50	1.99	560	119.9
C120-0	--	--	--	--	--	--	--	125.4
C120-400	6 No. 20	407	2.46	11.3	35	4.00	440	125.4
C120-500	6 No. 20	407	2.46	9.5	40	2.48	560	125.4

The spiral reinforcement was designed to meet the seismic design requirements of the 1994 CSA A23.3 Standard (CSA, 1994) and the 1995 ACI 318 Code (ACI, 1989) requirements, which are similar. Clause 10.9.4 of the 1994 CSA Standard requires that all spirally reinforced concrete columns contain a minimum ratio of volume of spiral reinforcement equal to:

$$\rho_s = 0.45\left(\frac{A_g}{A_c} - 1\right)\frac{f_c}{f_y} \tag{2.1}$$

where,

A_g = the gross area of concrete,

A_c = the area of the core of the column measured to the outside diameter of the spiral.

Clause 21.4.4.2 of the CSA Standard requires that ρ_s be not less than that given by:

$$\rho_s = 0.12 \frac{f'_c}{f_{yh}} \tag{2.2}$$

where,

f_{yh} = the specified yield strength of spiral reinforcement.

Equation 2.2 governs because the ratio A_g/A_c in Eq. 2.1 is less than 1.27. Although the CSA Standard requires that the spacing not exceed one-sixth of the core diameter, nor 75 mm, a practical maximum spacing of 100 mm was chosen in the C30 and C40 reinforced specimens even though Eq. 2.1 and Eq. 2.2 allowed for a larger spacing.

All fifteen specimens were cast vertically in *sonotube*, wax-coated cardboard tubes. Each series was cast separately with the concrete placed in three layers and thoroughly vibrated. The specimens were moist-cured in the forms for one week. After this sealed curing, the forms were stripped and cured at an ambient temperature of about 20° C and an average relative humidity of about 70%.

2.2 Material Properties

2.2.1 Longitudinal Reinforcement

The longitudinal reinforcing steel consisted of hot-rolled Grade 400 deformed bars satisfying CSA Standard G30.18-M (CSA, 1992). All longitudinal reinforcing steel was No.20 bars (A_s=300 mm^2, d_b=19.5 mm) and a weldable grade as required by CSA A23.3 for columns in ductile moment-resisting frames. The average values of the mechanical properties for the longitudinal bars were determined by testing three specimens at random and are summarized in Table 2.2. Figure 2.2 shows a typical stress-strain response of the longitudinal reinforcing steel bars.

Table 2.2: Average mechanical properties for No. 20 reinforcement bars

A_s (mm^2)	f_y (MPa)	ε_y (mm/mm)	f_u (MPa)
300	402	0.00201	656

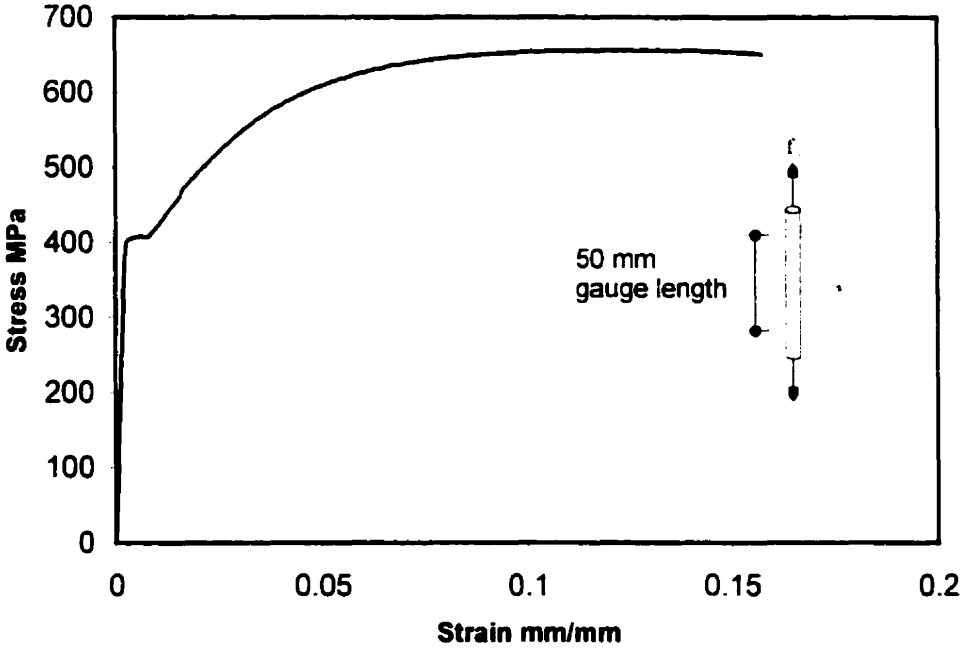

Figure 2.2: Typical stress-strain relationship for No.20 bars

2.2.2 Spiral Reinforcing Steel

Two types of spiral reinforcing steel were used, a Grade 400 hot-rolled deformed reinforcing bars and a Grade 500 cold-rolled deformed reinforcing bars. The bars were bent and coiled into spirals. The hot-rolled bars conform to the requirements of CSA Standard G30.18-M (CSA, 1992) and the cold-rolled reinforcement conforms to the requirements of CSA Standard G30.14-83 R1991 (CSA, 1991). The hot-rolled Grade 400 spirals were made from No.10 reinforcing bars (A_s=100 mm^2, d_b=11.3 mm). The cold-rolled Grade 500 spirals were made from #3 reinforcing bars (A_s=70.8 mm^2, d_b=9.5 mm). The average values of the mechanical properties of the spiral reinforcement were determined by testing three random samples and are summarized in Table 2.3. Figure 2.3 shows typical stress-strain relationships for the two types of spiral reinforcement. It is noted that the cold-rolled Grade 500 reinforcement has a considerably smaller ductility than the hot-rolled Grade 400 reinforcement. Unlike the longitudinal reinforcement, the Grade 400 steel used for the spirals has no distinct yield plateau.

Table 2.3: Average mechanical properties of the steel spiral

Grade	A_s (mm^2)	f_{yh} (MPa)	ε_y (mm/mm)	f_u (MPa)
400	100	410	0.0021	656
500	71	510	0.0025	697

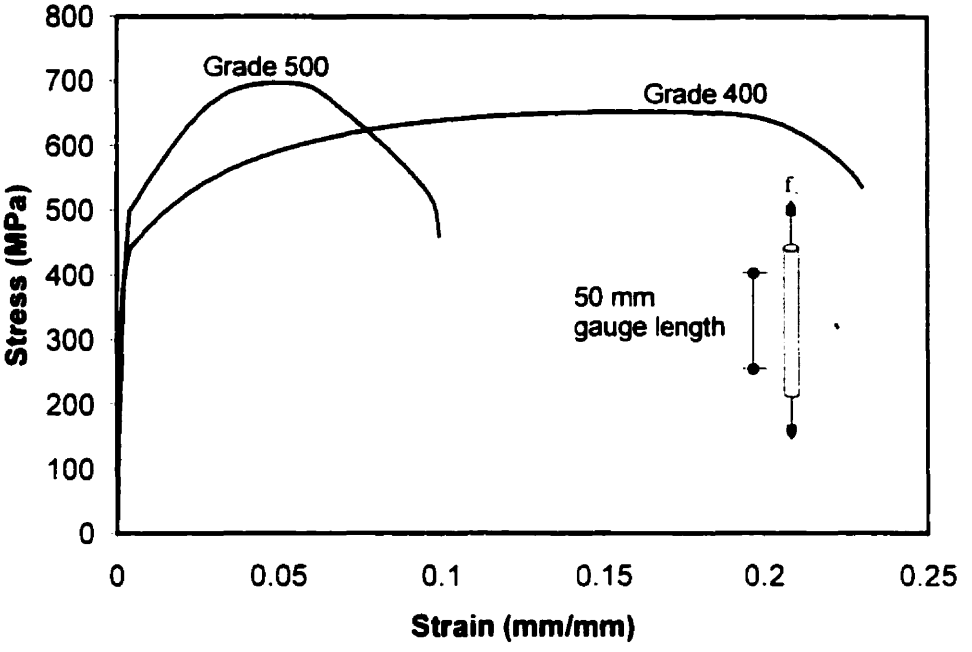

Figure 2.3: Steel spiral stress-strain responses

2.2.3 Concrete Properties

Five different strength concretes were used in this experimental program. Two series were produced at McGill University's Jamieson Structures Laboratory, the C30 and C60 series. The design mixes were obtained from a local ready-mix plant. The very high-strength concrete, the C100 and C120 series, were produced at the Civil Engineering Laboratories at the University of Sherbrooke. Finally, the concrete for the fifth series, the C40 series, was supplied by a local ready-mix plant. Table 2.4 describes the five concrete mixes used for this experimental program. Silica fume was used in the high-strength concrete series, C60, C100 and C120. A concrete slump of at least 200 mm was provided to ensure that the concrete could be placed through the congested reinforcing cages. The coarse aggregate consisted of limestone with a maximum aggregate size of 20 mm for the C30 and C40 concrete, and a maximum aggregate size of 10 mm for the C60, C100 and C120 concrete. All specimens were cured as described in Section 2.1. Figure 2.4 shows the representative concrete stress strain responses in compression.

Table 2.4: Concrete mix designs

Specified Concrete Strength		30	40	60	100	120
Cement	(kg/m^3)	355[1]	318[2]	470[3]	540[3]	500[4]
Silica Fume	(kg/m^3)	--	--	(35.25)[5]	(40.5)[5]	55
Fine Aggregate	(kg/m^3)	790	837	741	720	840
Coarse Aggregate	(kg/m^3)	1040	1119	1063	1100	1050
Water	(L/m^3)	178	125	135	114	100
Water-Cement Ratio		0.5	0.39	0.29	0.25	0.19
Water Reducer	(mL/m^3)	1110	1057	1471	--	--
Air-Entraining Agent	(mL/m^3)	180	129	480	--	--
Superplasticizer	(L/m^3)	--	--	11	22.8	22.2
Retardent	(mL/m^3)	--	--	600	750	--

(1) Type 10 cement

(2) Type 30 cement

(3) Type 10SF cement

(4) Type 50 cement

(5) Quantity already included in Type 10SF cement

A series of standard cylinders and flexural beams were prepared from each of the five concrete batches and tested to determine the concrete properties. These specimens had identical curing to the column specimens, as described in Section 2.1. The compressive strength and split-cylinder tests were each determined from three 150 mm diameter by 300 mm cylinders from each batch. From the compression tests the following properties were obtained: the concrete compressive strength f'_c, the peak strain ϵ_{co}, and the modulus of elasticity, E_c. The secant modulus of elasticity was calculated as the slope of the secant of the stress-strain curve at 0.4 f'_c, on the ascending part of the curve. The split-cylinder test was used to obtain the splitting tensile stress, f_{sp}. The modulus of rupture, f_r, was determined by subjecting the flexural beams to a three point loading test. The flexural beams had nominal dimensions of 150 x 150 x 600 mm. Table 2.5 gives the average values of the material properties obtained from three samples, along with the standard deviation of these properties.

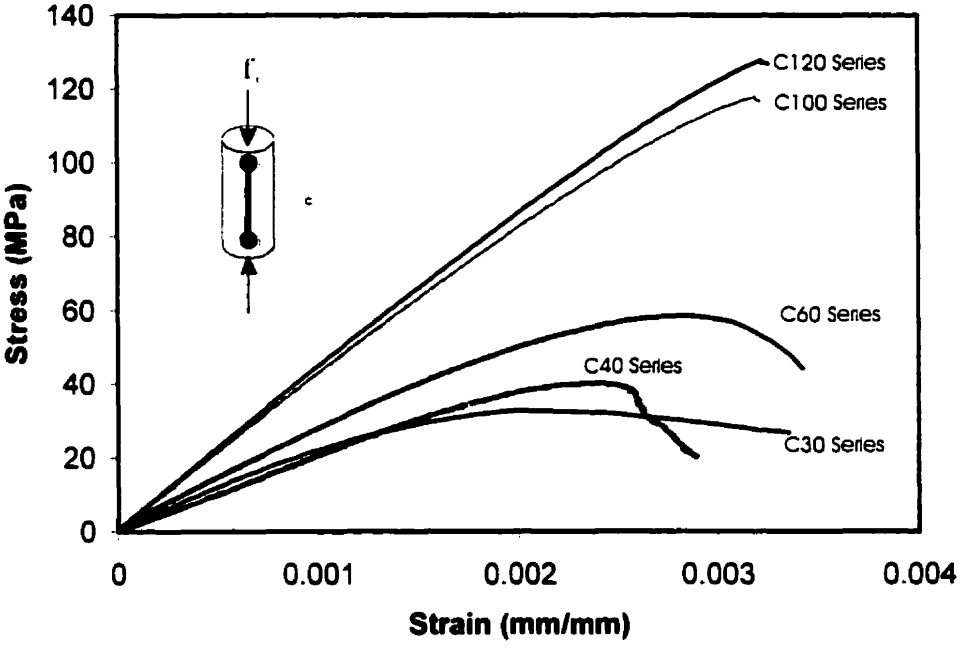

Figure 2.4: Concrete stress-strain responses

Table 2.5: Concrete Properties

Series	f'_c (MPa)	ε_{co} (mm/mm)	f_r (MPa)	f_{sp} (MPa)
C30	35.5	0.00302	4.31	2.52
(std. Deviation)	(2.46)	(0.00145)	(0.02)	(0.21)
C40	39.5	0.00232	4.62	2.94
(std. Deviation)	(0.68)	(0.000011)	(0.28)	(0.15)
C60	59.5	0.00262	4.28	3.41
(std. Deviation)	(1.07)	(0.0018)	(0.30)	(0.03)
C100	119.9	0.00320	10.36	7.15
(std. Deviation)	(2.03)	(0.00002)	(0.19)	(0.08)
C120	125.4	0.00339	9.37	7.2
(std. Deviation)	(1.94)	(0.00123)	(0.74)	(0.23)

For each concrete type, two shrinkage specimens were cast along with the cylinder and flexural beam specimens. Each standard shrinkage specimen was 50 mm x 50 mm with a 280 mm gauge length. Readings were taken periodically between two metal studs embedded in the shrinkage specimens. Figure 2.5 shows the average shrinkage versus time responses of the shrinkage specimens for the concrete from each series.

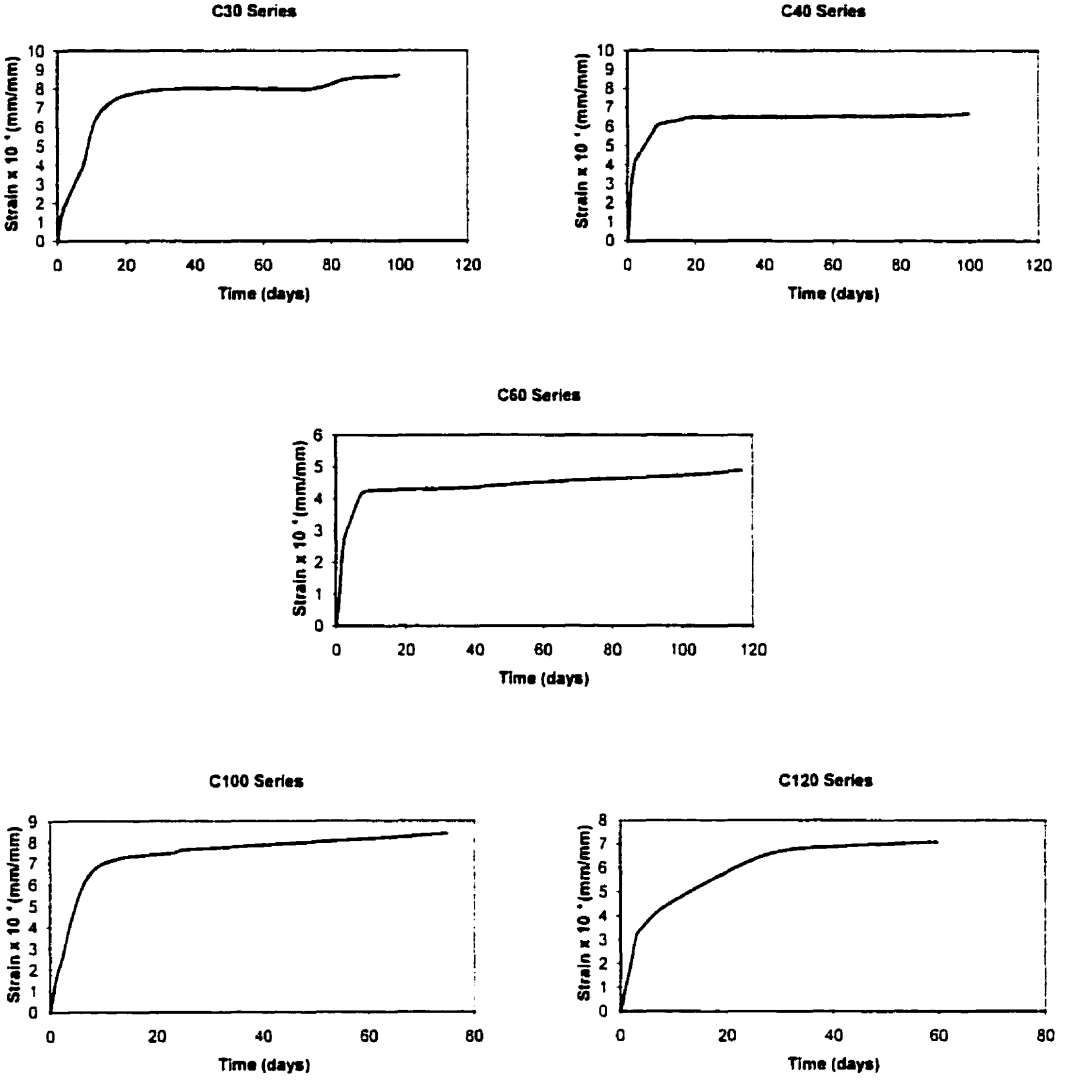

Figure 2.5: Variation of concrete shrinkage strains with time

2.3 Test Setup

All specimens were tested under the 11400 kN capacity MTS universal testing machine in the Department of Civil Engineering Structures Laboratory at McGill University. The specimens were placed vertically on top of a three inch thick steel plate. A one inch steel bearing plate was placed on the top of the specimen. Special attention was taken to ensure that the specimens were aligned vertically to eliminate loading eccentricities. A thin layer of grout was placed both on the bottom and top of the each specimen to ensure a proper bearing surface.

Steel collars were place at the top and bottom of each specimen. The collars were fabricated from one half-inch thick, twelve inch diameter steel pipe. See Fig. 2.6 for collar details. These collars were used to provide additional confinement at the top and bottom of the specimens. At each end of the specimen, a 10 mm gap was provided between the steel collar and the end steel bearing plate. This ensured that the steel collar would not bear against the steel plate.

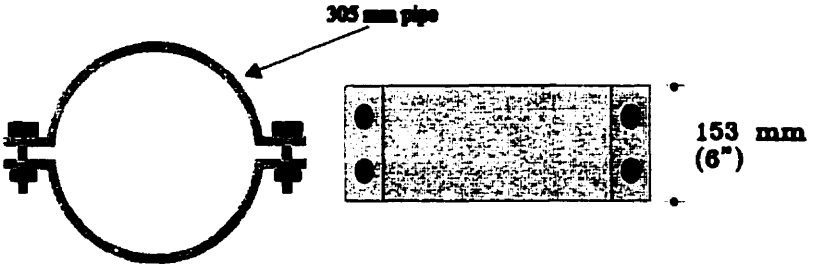

Figure 2.6: Specimen confinement collar

Special precautions were taken for the plain concrete specimens. It was anticipated that the plain specimens would fail abruptly and have little structural integrity. As a safety precaution for the plain concrete tests, the steel collars were fitted with steel plates to attach a steel wire connecting the top of the column specimen to the head of the testing machine.

2.4 Instrumentation

The response of each specimen was monitored continuously throughout the test by a computerized data acquisition system. The data acquisition system measured the load from the load cell, displacements from the Linear Voltage Differential Transducers (LVDT's) and strains from the electrical resistance strain gauges at frequent intervals of applied load.

There were two LVDT configurations, one configuration for the six ultra high-strength specimens and another configuration for the other specimens.

The lower strength specimens have eight vertical LVDT's as shown in Fig. 2.7. Three LVDT have gauge lengths of 1400 mm while the other five LVDT's have gauge lengths of 280 mm. The three full-length LVDT's were attached to the steel collars at the bottom of each specimen to determine the average strains over the height of the column specimens. The LVDT's with the shorter gauge lengths were attached to threaded rods embedded in the concrete specimen in order to determine the strains in different segments over the column height.

Four vertical LVDT's were used for the six ultra high-strength concrete specimens (series C100 and C120) as shown in Fig. 2.8. All four LVDT's had a gauge length of 1400 mm. The shorter gauge length LVDT's were not used on these very high-strength concrete columns because there was concern that the holes for the threaded rods may affect the strength.

Strains were measured by the use of electrical resistance strain gauges. Two electrical resistance strain gauges, having a gauge length of 2 mm, were glued to the lateral confining spiral steel at the column mid-height, 180 degrees apart, as shown in Fig. 2.9. These electric resistance strain gauges were used to monitor the strain of the spiral steel of the spiral reinforcement.

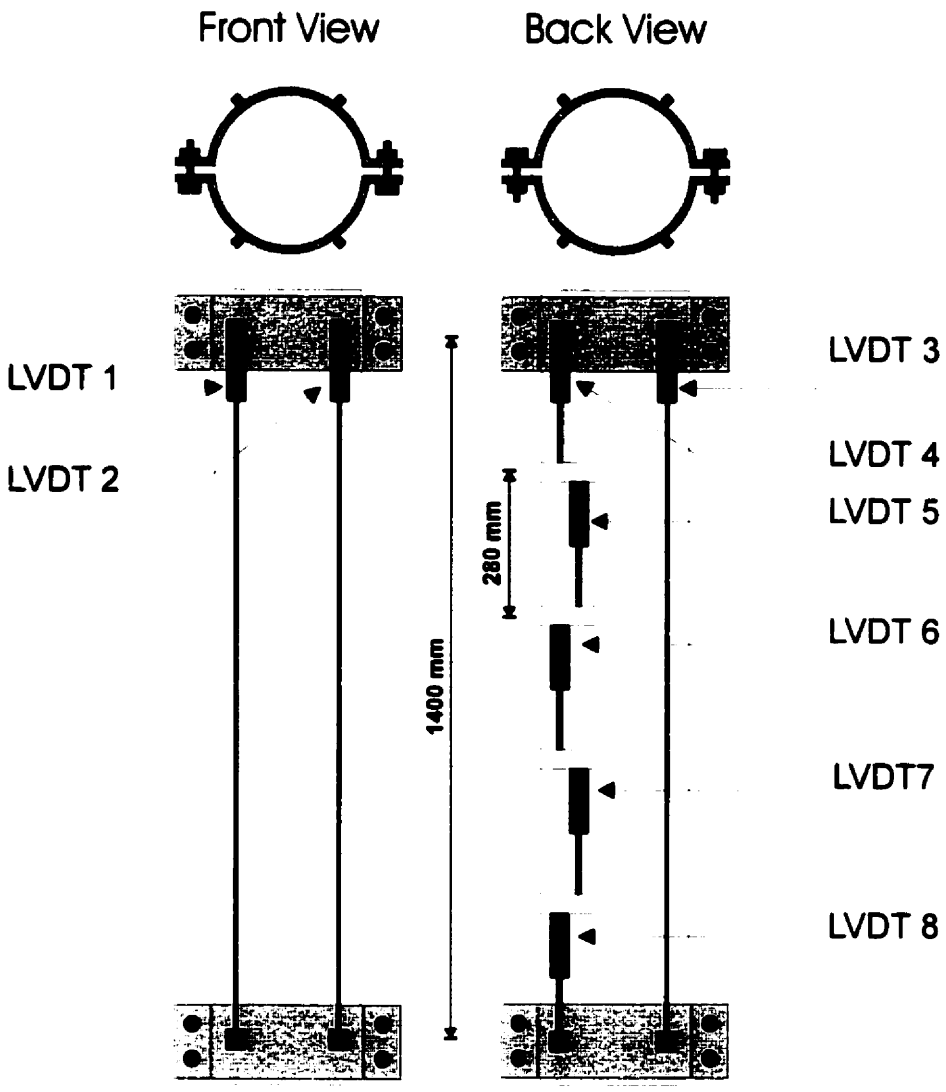

Figure 2.7: LVDT configuration for C30, C40, and C60 series

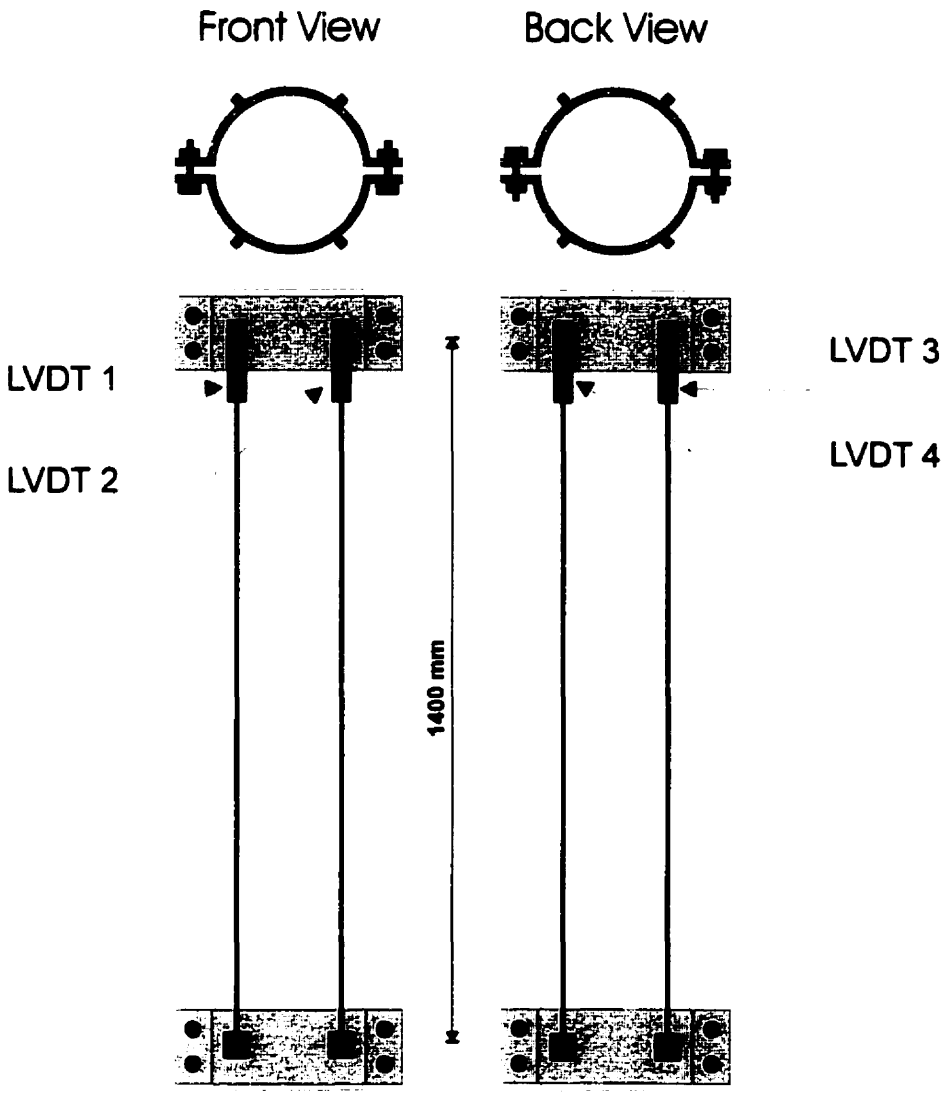

Figure 2.8: LVDT configuration for C100 and C120 series

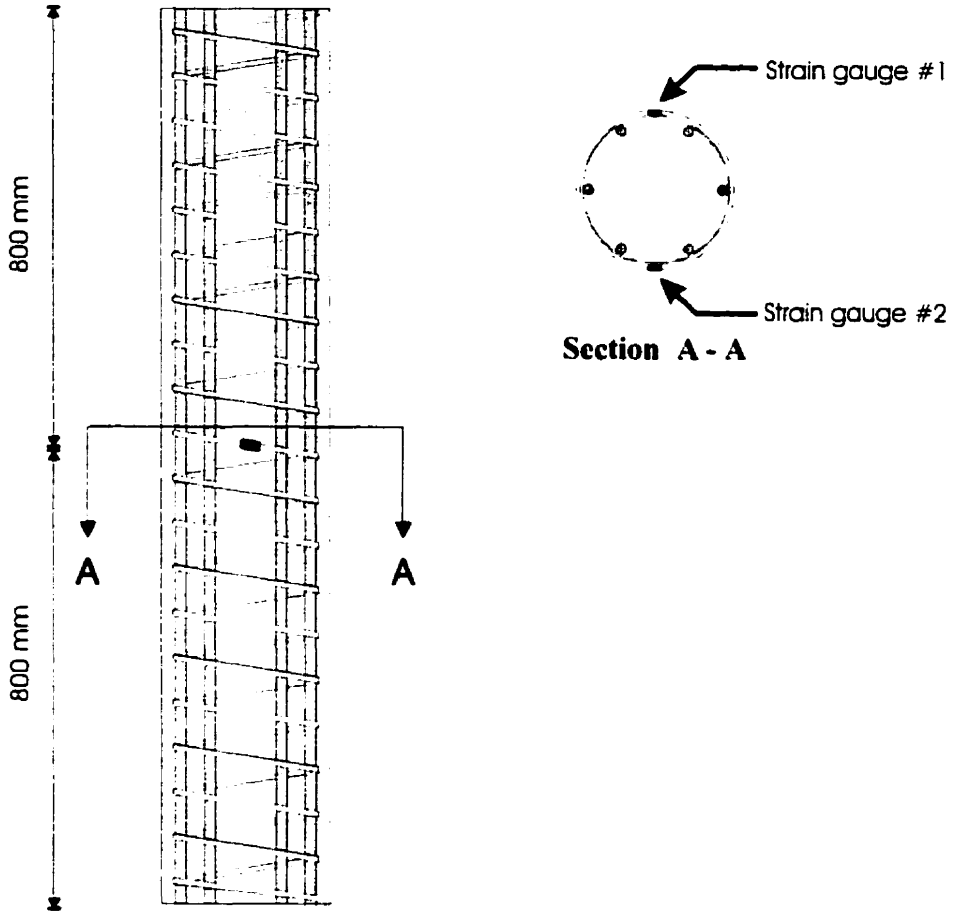

Figure 2.9: Location of electric resistance strain gauges

2.5 Test Procedure

All fifteen specimens were tested in the same manner. The MTS machine was used to apply load at a slow rate to avoid dynamic affects. A loading rate of 0.003 mm/sec was used throughout the test. The loading was applied until the failure of the plain concrete columns, whereas the reinforced concrete columns were loaded beyond the deflection corresponding to their maximum load. The reinforced columns were loaded until the specimen was only able to carry 50% of it peak load. The duration of each test was approximately three hours for the reinforced specimens and one hour for the plain specimens.

Chapter 3

Experimental Results

3.1 Introduction

In this chapter the behaviour of the fifteen column specimens is presented. The results of this experimental program are presented in six sections, one section for the five plain concrete specimens, and a separate section for each of the five reinforced concrete column series. In addition, comparisons will be made between the three column specimens in each series. For the lower strength series, C30, C40, and C60 figures are included showing the distributions of longitudinal strain over the full height of the column. On each figure, the gray shaded segments indicate the load-strain response in that particular segment of the column. The energy absorption capacity of the reinforced columns is also compared.

The energy absorption capacity of the reinforced column specimens will be measured by comparing the area under the load-strain curve and by comparing the specimen's longitudinal strain at the point where the load carrying capacity of the specimen falls to 50% of the peak load on the descending branch of the load-strain response. The area will be computed by numerical integration from zero strain until the strain at 50% of peak load on the descending branch. The area under the load-strain response curve provides a measure of the toughness of each column.

3.2 Response of Plain Concrete Specimens

Five plain column specimens were tested, having nominal compressive strengths of 30, 40, 60, 100, and 120 MPa. Figures 3.1 through Fig. 3.5 show the load-strain responses for each of the five plain column specimens. Note that only the first three column specimens have plots of the longitudinal strain distribution over the height of the column. The two ultra

high-strength plain concrete column specimens did not include local strain measurements for the reasons mentioned in Section 2.4.2. Table 3.1 compares the peak load and corresponding strain for each of the five plain concrete specimens. Figure 3.6 compares the load-strain response of all five plain column specimens.

Specimens C30-0 and C40-0 both failed in a manner similar to the failure of a standard concrete test cylinder in a compression test. These two plain columns failed in a relatively gradual manner rather than in an abrupt brittle failure. Therefore, both specimens still had some degree of structural integrity after reaching their peak loads. Specimen C40-0 reached its peak load at a strain of 0.00207, while Specimen C30-0 reached its peak load at a strain of 0.0032. The strain at the peak load of Specimen C40-0 was over 30% smaller than that of Specimen C30-0.

Table 3.1: Summary of Results for the Plain Concrete Specimens

Specimen	Peak Load (kN)	Strain at peak (mm/mm)
C30-0	2368	0.00320
C40-0	2861	0.00207
C60-0	3278	0.00254
C100-0	5414	0.00327
C120-0	6859	0.00309

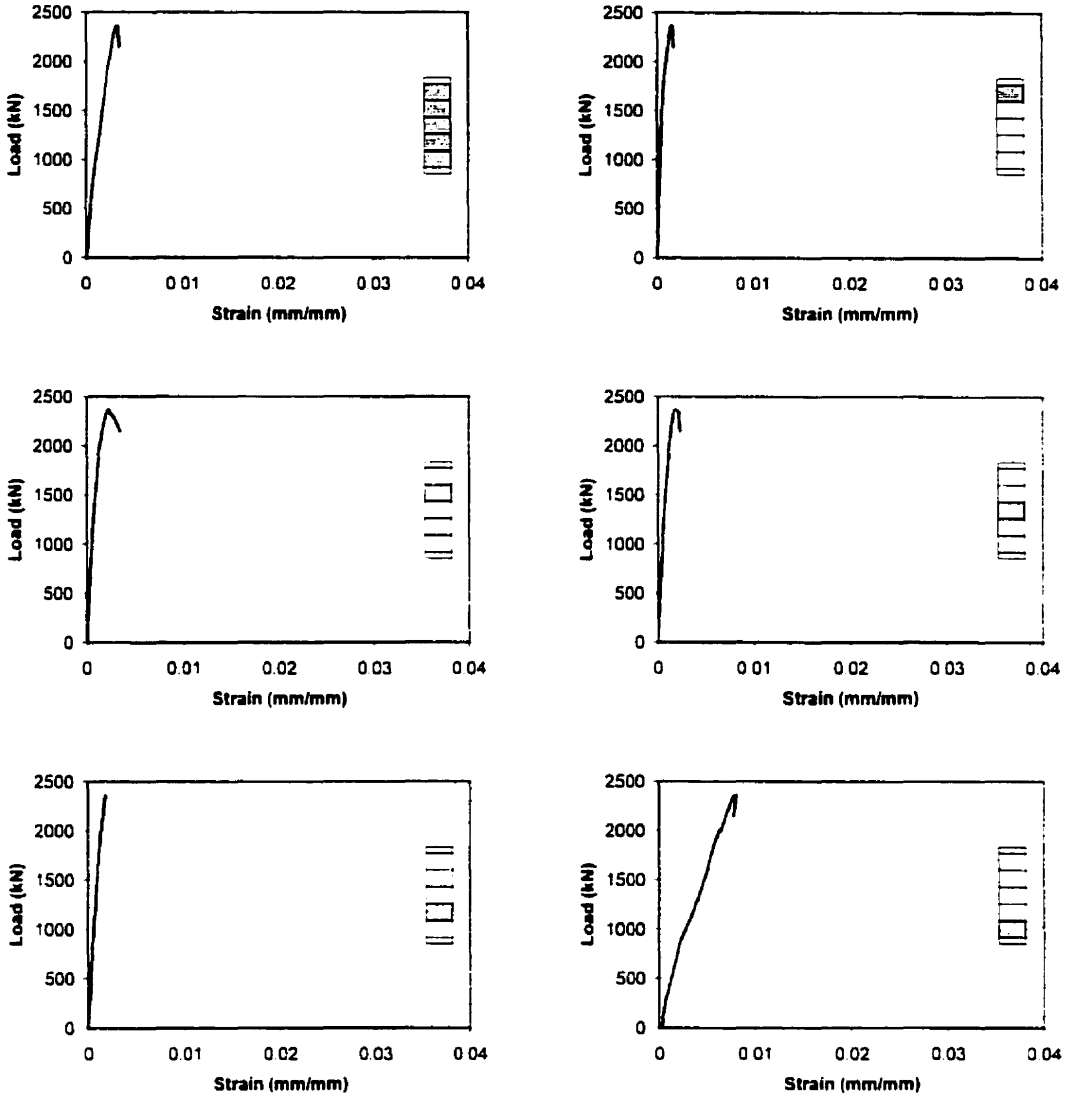

Figure 3.1: Load-strain response of C30-0

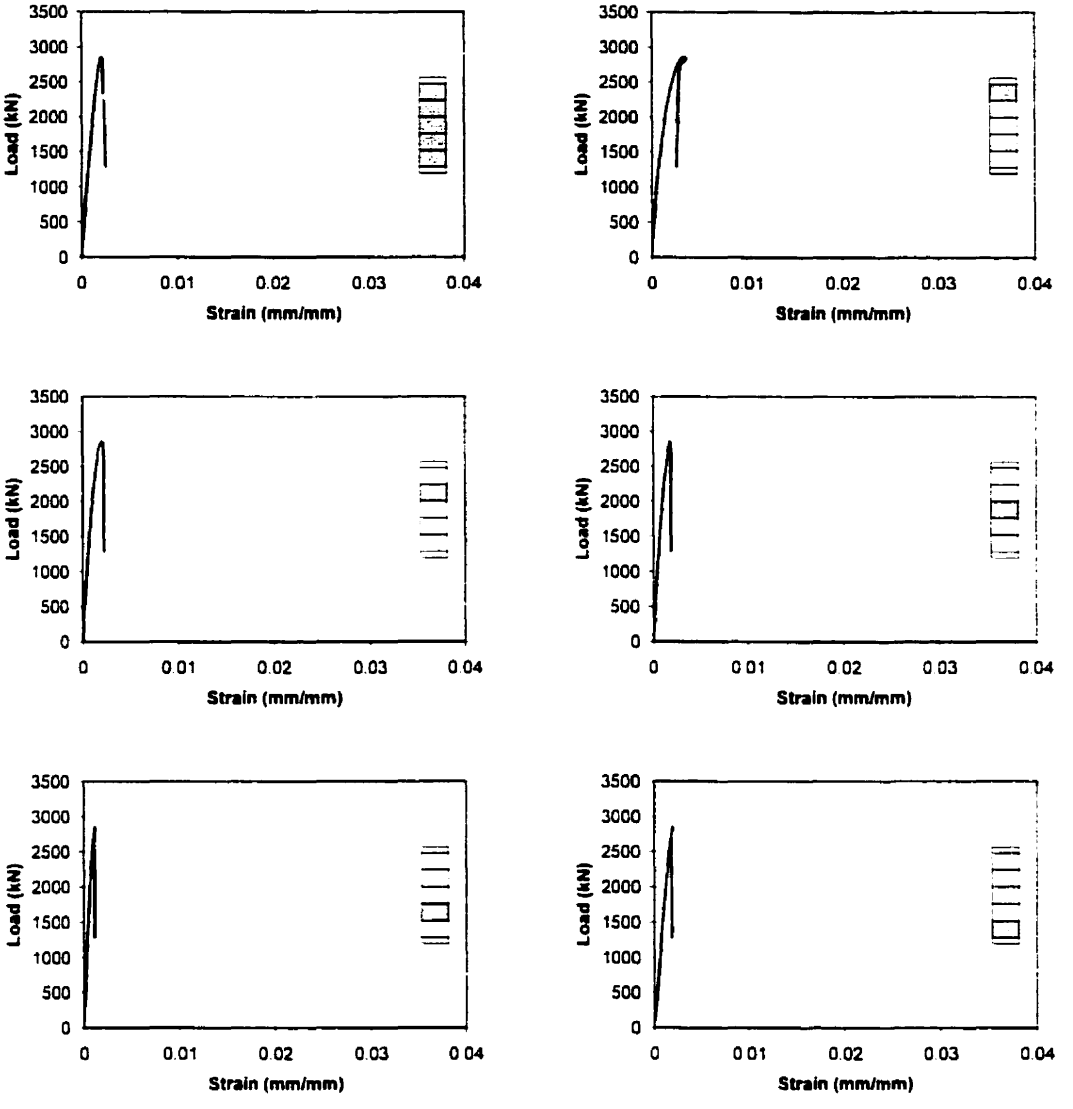

Figure 3.2: Load-strain response of C40-0

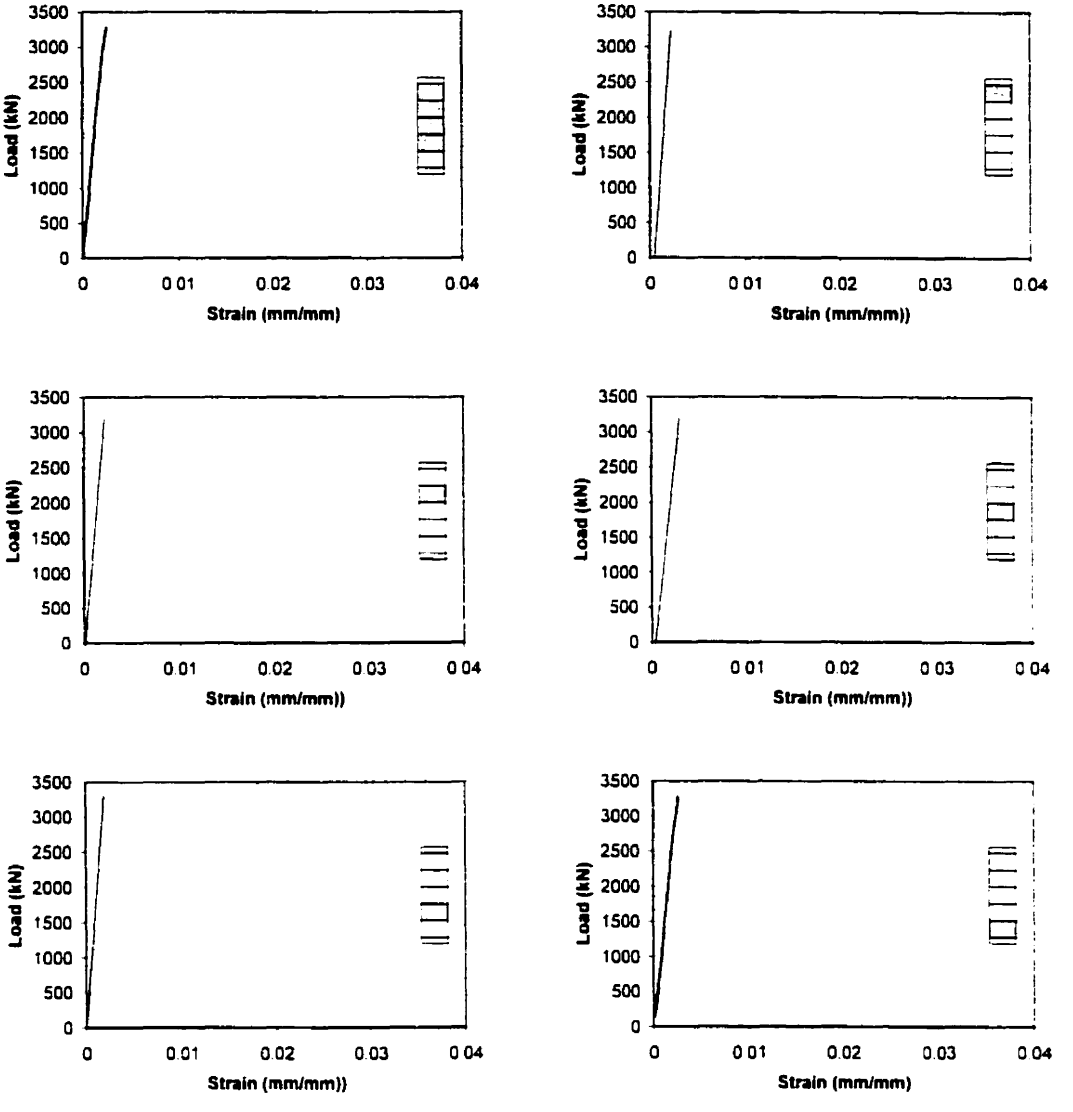

Figure 3.3: Load-strain response of C60-0

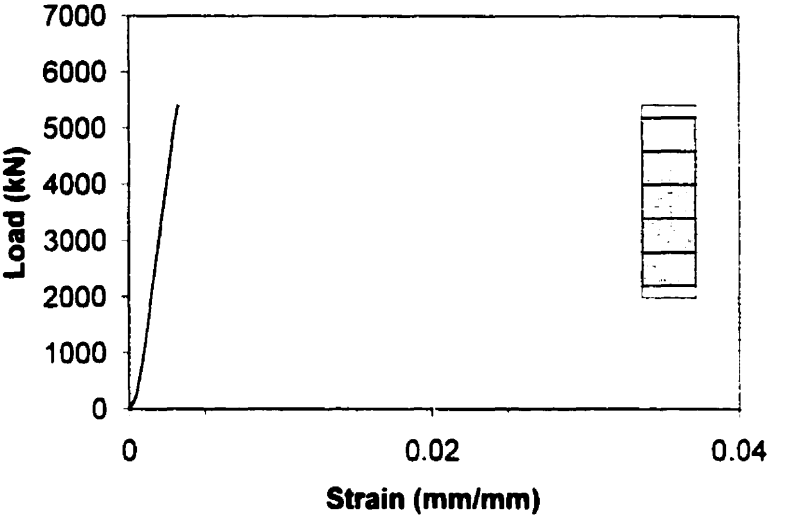

Figure 3.4: Load-strain response of C100-0

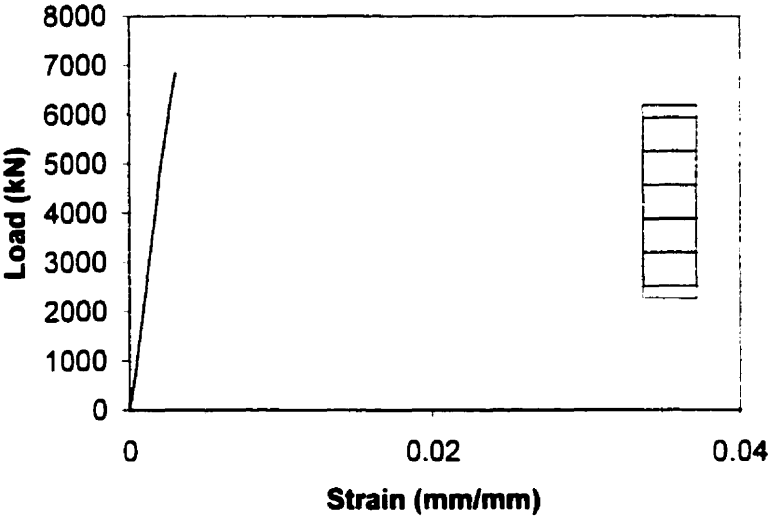

Figure 3.5: Load-strain response of C120-0

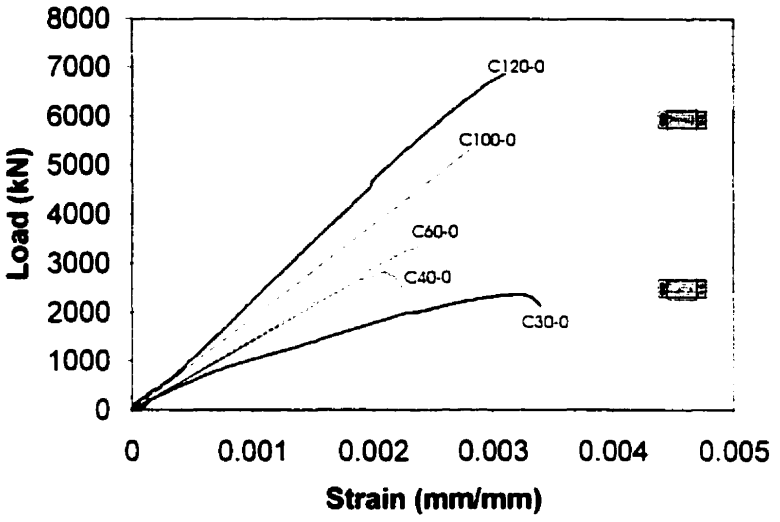

Figure 3.6: Plain specimens load-strain responses

Specimen C60-0 showed no ductility when compared to Specimen C30-0 or C40-0. It did not have a descending branch on the compressive load-strain response. The failure was somewhat explosive. A 5 kg fragment of the concrete specimen exploded at failure and traveled over two metres. Due to the explosive nature of this specimen's failure, there was no structural integrity after the peak load was reached. The failed specimen fractured into two equal parts. Specimen C60-0 failed with an average longitudinal strain of 0.00254, measured along the full height. As with Specimen C40-0, the strain was lower than the average concrete crushing strain obtained from the standard cylinder tests. Figure 3.3 shows that the strains in all five segments were close to uniform.

The high-strength plain concrete specimens, C100-0 and C120-0 were extremely brittle with load-strain curves exhibiting a linear response with no post-peak resistance. Although no ductility was observed, both specimens exhibited warning signs that suggested that their failure was imminent. A longitudinal splitting crack over the full height of each column developed. The crack width was about 1 mm. Both specimens failed in violent explosions. Figure 3.7 shows a photograph of Specimen C100-0 after failure. Specimen

C100-0 still had some structural integrity even though over half of its cross-sectional area had been lost. The failure of Specimen C120-0 was more extreme than that of Specimen C100-0. Two vertical cracks about 50 mm apart formed over the entire height of the specimen. After Specimen C120-0's explosive failure, only the concrete between the vertical cracks remained. This failure released so much energy that the steel circular collar was deformed into an ellipsoid shaped collar. The strains at failure for Specimens C100-0 and C120-0 are similar, 0.00327 versus 0.00309, respectively. Figure 3.8 shows a photograph of Specimen C120-0 after failure.

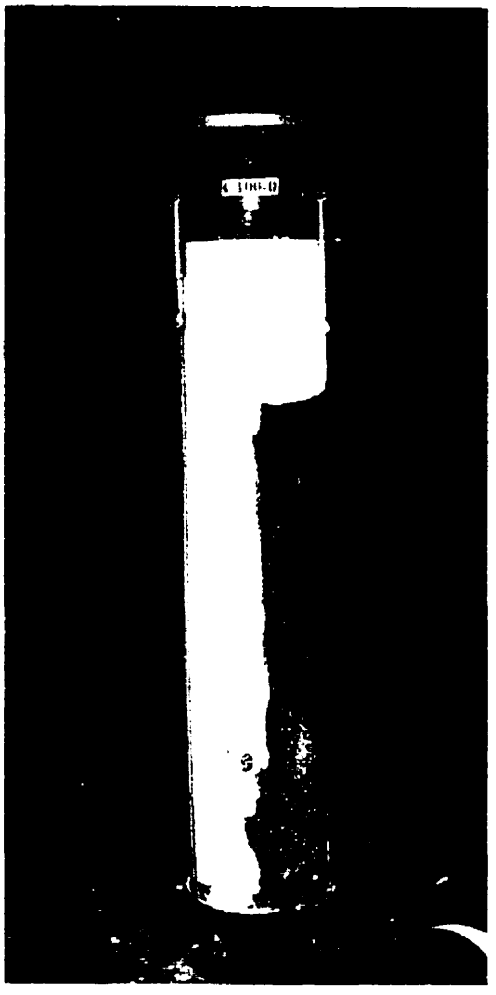

Figure 3.7: Specimen C100-0 at failure

Figure 3.8: Specimen C120-0 at failure

3.3 Summary of Results for the Reinforced Column Specimens

Table 3.2 shows test results of the reinforced specimens obtained from the experimental procedure discussed in Section 2.3. The following information is given:

A_{50} = area under the load-strain curve integrated from $\varepsilon = 0$ until $\varepsilon = \varepsilon_{C50C}$.

P_{max} = peak load carried by the specimen,

ε_{cc} = axial strain of confined concrete corresponding to the peak load.

ε_{C50C} = axial strain in confined concrete corresponding to the point where the load dropped to $0.5P_{max}$ on the descending branch.

ρ_s = ratio of transverse reinforcement in column cross-section.

Table 3.2: Summary of responses for the reinforced specimens

Specimen	ρ_s (%)	P_{max} (kN)	ε_{cc} (mm/mm)	ε_{C50C} (mm/mm)	A_{50} (kN)
C30-400	1.40	2789	0.004864	0.0175	40.69
C30-500	1.00	2771	0.002379	0.0810	19.3
C40-400	1.40	3893	0.003233	0.0145	41.43
C40-500	1.00	3984	0.004329	0.0083	24.68
C60-400	1.86	3982	0.003795	0.0155	46.13
C60-500	1.24	4024	0.004021	0.0083	24.45
C100-400	3.11	6222	0.00576	0.0201	84.13
C100-500	1.99	6598	0.004978	0.0081	42.19
C120-400	4.00	7303	0.009054	0.0303	102.99
C120-500	2.48	7611	0.007557	0.0132	44.13

3.4 Response of C30 series

The C30 series was instrumented with 8 LVDT's and 2 strain gauges as shown in Fig. 2.7 and Fig 2.9. The results are summarized in Table 3.2.

3.4.1 Response of Specimen C30-400

Specimen C30-400 behaved in a ductile manner. The strain at failure of Specimen C30-400 was about eight times that of the plain concrete specimen. Cracking began at the center of the specimen, but had little affect on the specimen's response until the load reached 2603 kN at an average strain of 0.00295. At this point the concrete cover spalled off. Although the load did not drop at this point, a noticeable change in the slope was apparent on the load-strain curve (see Fig.3.9). The specimen's load carrying capacity continued to increase until a peak load of 2787 kN was reached at an average strain of 0.00501, thus exhibiting significant post-spalling behaviour. This 187 kN increase in load carrying capacity after spalling can be attributed to the confining effect of the spiral reinforcement. After the peak, the load carrying capacity of the specimen dropped at an approximately constant rate until the buckling of the vertical bars ended the test. The steel spiral did not rupture and thus remained fully effective throughout the test.

The stress in the steel spiral never reached the ultimate stress because the strain in the steel spiral remained considerably below that of the rupture strain. The two strain gauges on the spiral reinforcement were 180° apart and at about the same elevation. However, these gauges showed significantly different strains (see Fig.3.10). One strain gauge indicated that the spiral had yielded, while the other strain gauge indicated that the spiral did not yield. The strains in the spiral decreased after the peak load. This is attributed to a relaxation effect due to the longitudinal bar buckling. As soon as the longitudinal bars began to buckle, the strain in the spiral decreased.

The strains at different sections in Specimen C30-400 are shown in Fig 3.11. From these plots it is easy to see where the failure occurred. The strain response measured by LVDT 5 was far greater than the strains of all the other LVDT's. A decrease in strain in the neighboring LVDT's was also recorded after the peak load was reached.

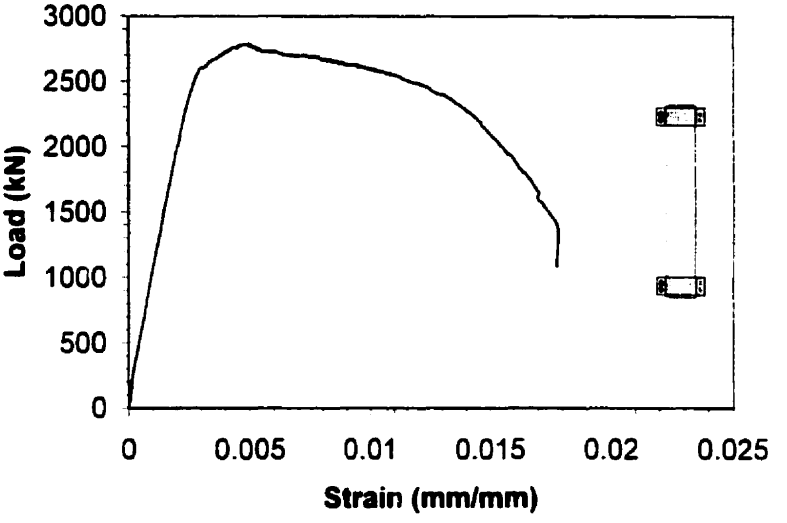

Figure 3.9: Average load-strain response for C30-400

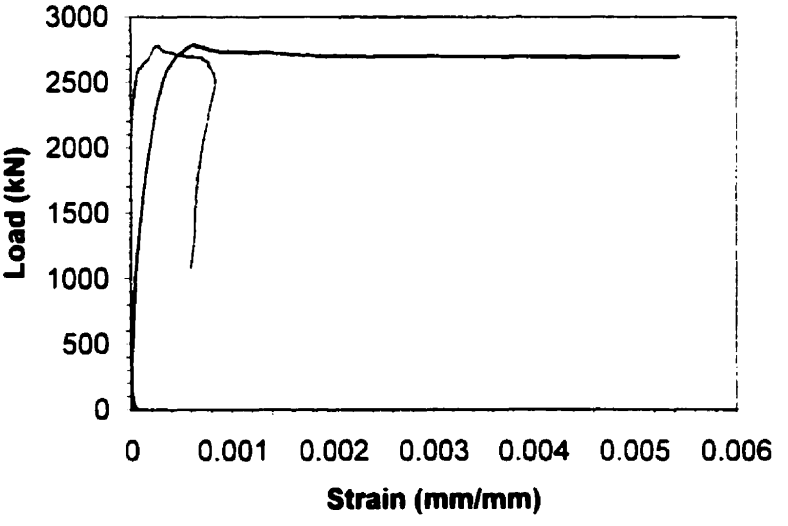

Figure 3.10: Spiral reinforcement strains for C30-400

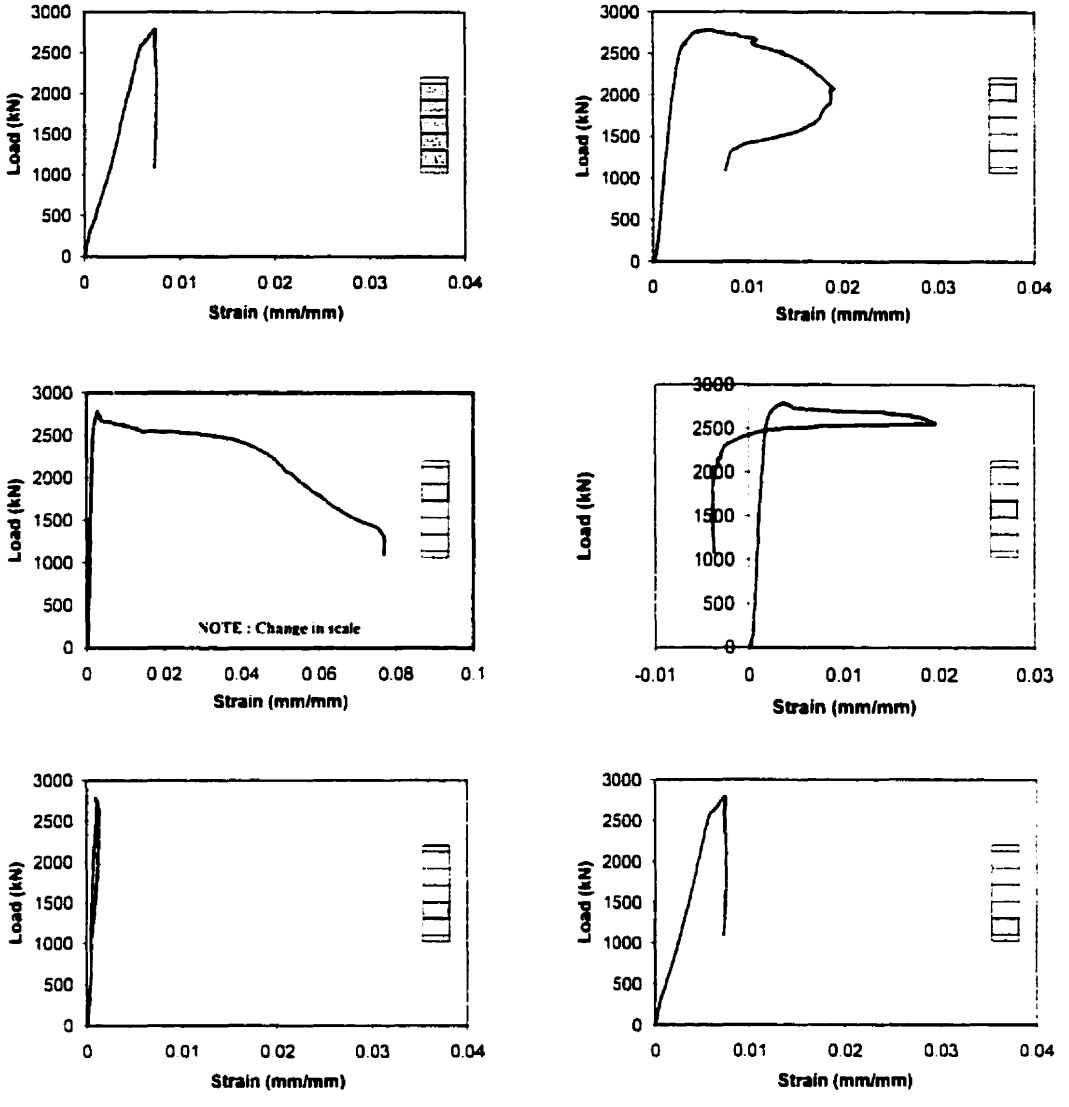

Figure 3.11: Load-strain responses of C30-400

3.4.2 Response of Specimen C30-500

Specimen C30-500 also behaved in a ductile manner. The first cracks appeared slightly below the top steel confining collar. However, these initial cracks soon spread downward and continued increasing in size and number until spalling occurred throughout the specimen. Specimen C30-500 continued to carry additional load until a peak load of 2771 kN was reached at an average strain of 0.0024. No clearly defined post-peak behavior was noticed. Spalling occurred progressively until the peak load was reached. Figure 3.12 shows the load-strain response for Specimen C30-500. After reaching the peak load, the load dropped slightly and then remained relatively constant, indicating that the spiral steel had not yet yielded. When a longitudinal strain of 0.0063 was reached, the load carrying capacity of the specimen began to decay at an accelerated rate, indicating that the spiral had yielded. This decay in the specimen's load carrying capacity continued until the spiral ruptured. The first rupture occurred at an average longitudinal strain of 0.008. A second rupture quickly followed at an average strain of 0.0081. Both spiral steel ruptures occurred near each other at approximately the same column height. Both failures occurred near the vertical bars, due to additional stress on the steel spiral caused by the buckling vertical bars.

The failure in this test occurred at the top of the specimen, away from strain gauges at mid-height. The spiral reached only half-yield at mid-height. Therefore, there was a large variation in the spiral's stress. Figure 3.13 shows the strain gauge readings for Specimen C30-500. Where the steel spiral ruptured, an ultimate stress of 697 MPa was reached, whereas only a stress of about 280 MPa (about half-yield) was measured by the strain gauges at the specimen's mid-height. Once the specimen began to fail due to concrete crushing, the strain in the steel spiral decreased.

Figure 3.14 shows the strains at the different sections of Specimen C30-500. Once again the post-peak strain is highly localized. The strains are uniform until the peak load is reached, but once the peak load is reached, only the strains in the two top segments continue to increase, while the strains in the bottom three segments remain constant.

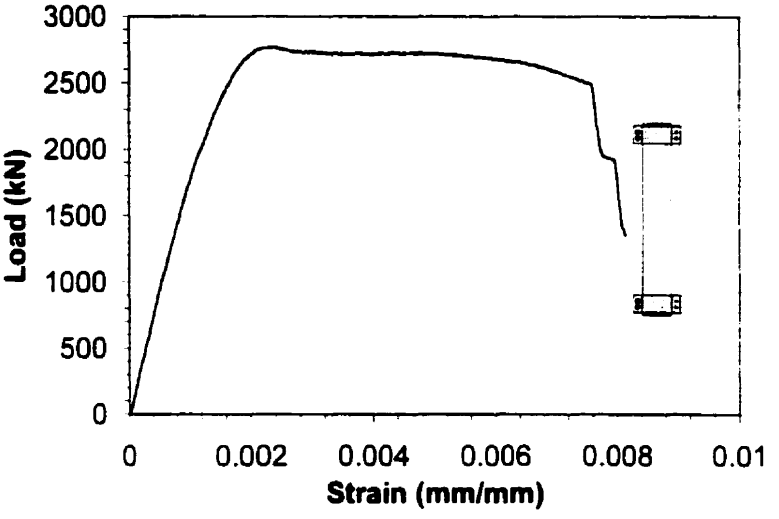

Figure 3.12: Average load-strain response for C30-500

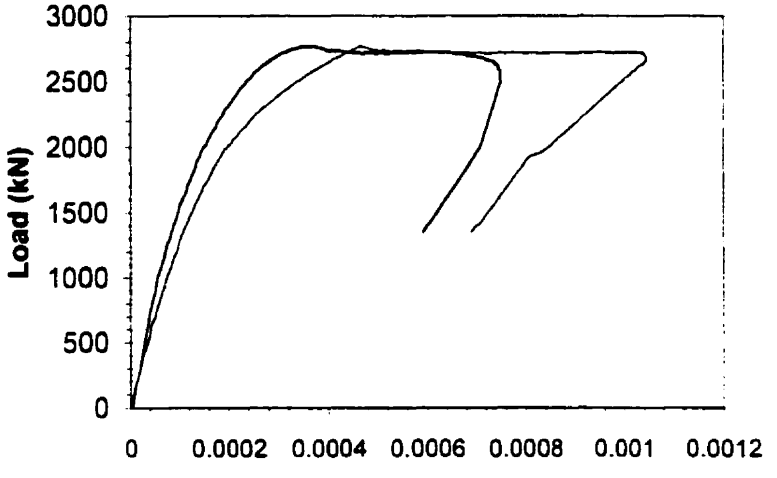

Figure 3.13: Spiral reinforcement strains for C30-500

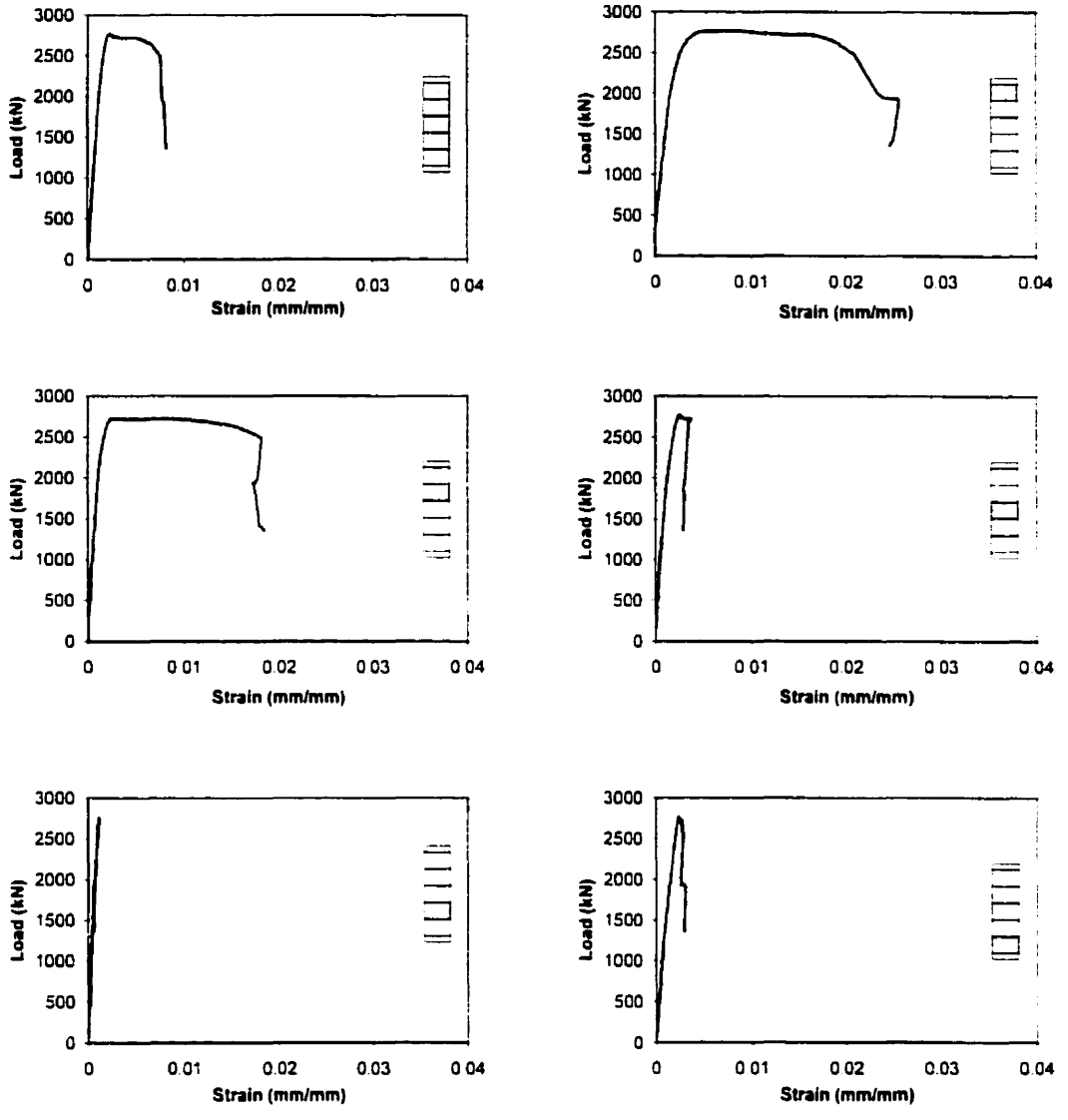

Figure 3.14: Load-strain responses of C30-500

3.4.3 Comparison of C30 Series

Both reinforced specimens behaved similarly up to a longitudinal strain of 0.008. Figure 3.15 shows a plot of both specimens, and Fig. 3.16 shows a photograph of both specimens following the test. Specimen C30-400 was twice as ductile as Specimen C40-500. The areas under the load-strain curves for Specimens C30-400 and C30-500 are 40.69 kN and 19.30 kN, respectively. This large difference in column ductility is attributed to the fact that the Grade 500 steel was much less ductile than the Grade 400 steel (see Fig 2.3).

The peak load from both specimens was approximately the same. However, the C30 specimens did behave differently prior to the peak load. Specimen C30-400 has a well-defined point at which spalling began, while Specimen C30-500 only showed a slight change in slope where spalling began. After the spalling of the concrete cover, both specimens gained load due to the confinement provided by the spiral, but the increase in load in Specimen C30-400 was more significant.

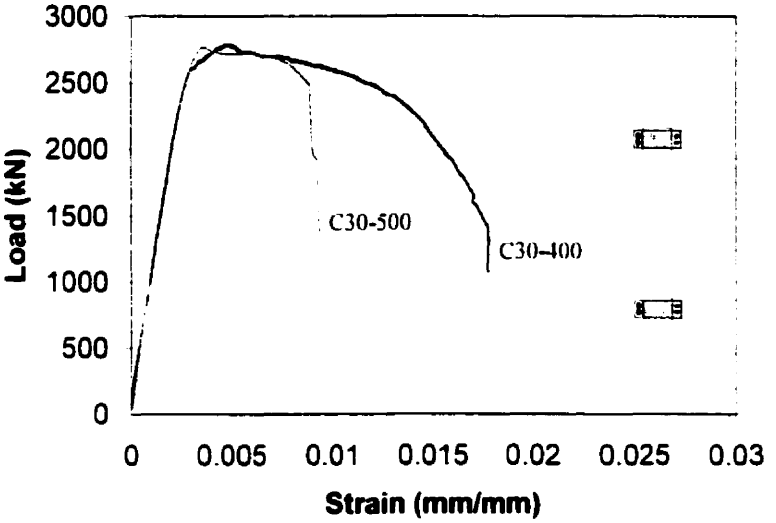

Figure 3.15: Load-strain response for C30 series

Figure 3.16: Photo of C30-400 and C30-500 at failure

3.5 Response of C40 series

The C40 series was instrumented with 8 LVDT's and 2 strain gauges as shown in Fig. 2.7 and Fig. 2.9. The results are summarized in Table 3.2.

3.5.1 Response of Specimen C40-400

The load-strain response for Specimen C40-400 is shown in Fig. 3.17. Cracking in the concrete cover began when the load reached 3750 kN. This initial cracking began near the top steel confining collar and quickly spread downward throughout column. The spalling of the concrete cover began when a load of 3808 kN at an average longitudinal strain of 0.0029 was reached. This point is not as well defined as that of Specimen C30-400. with only a slight change of slope being identified in Specimen C40-400. The slope of the load-strain response changed from a linear response to parabolic response. This increase in the specimen's load carrying capacity was due to the confining effects of the spiral steel. A peak load of 3893 kN at an average longitudinal strain of 0.00323 was reached. After the peak load was reached. the load carrying capacity of the column dropped at an approximately linear rate until the specimen failed. The failure of Specimen C40-400 was caused by the buckling of its vertical reinforcement bars. The spiral did not rupture in this test.

Since the steel spiral did not rupture in this test. the ultimate stress of the spiral was not reached anywhere in the specimen. The two strain gauges on the specimen showed only a slight strain in the steel spiral at mid-height. Although. the stress in the steel spiral at mid-height was less than half of its yield stress. it is likely that a higher stresses in the spiral reinforcement were present where crushing in the concrete occurred.

Figure 3.19 shows the longitudinal strain of the five segments of the column specimen. The strains in all five segments were approximately equal until crushing. Once

again, most of deflection after the initial crushing occurred in the segment of the specimen that the crushing of the concrete occurred.

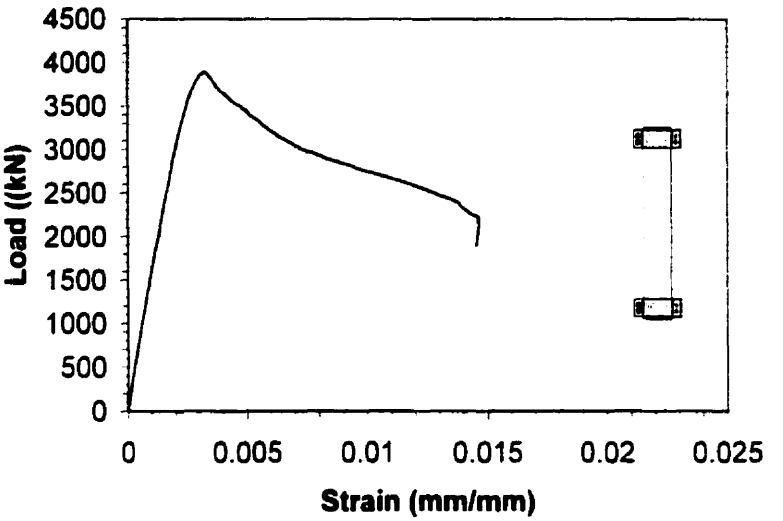

Figure 3.17: Average load-strain response for C40-400

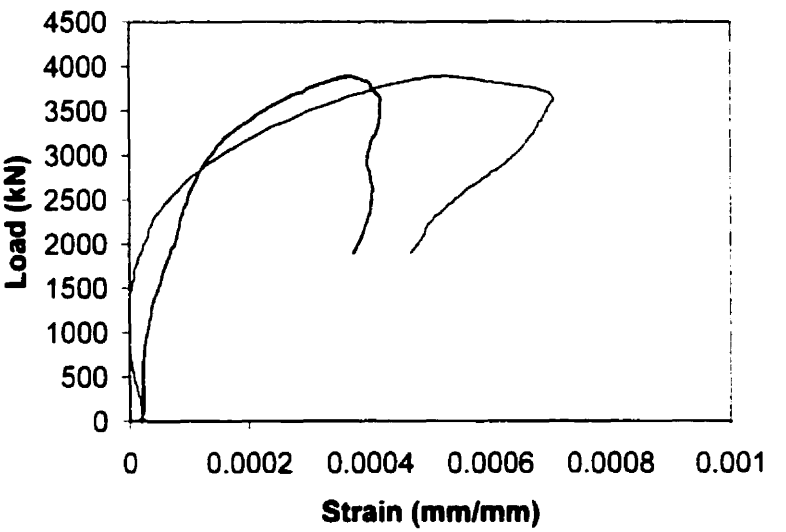

Figure 3.18: Spiral reinforcement strains for C40-400

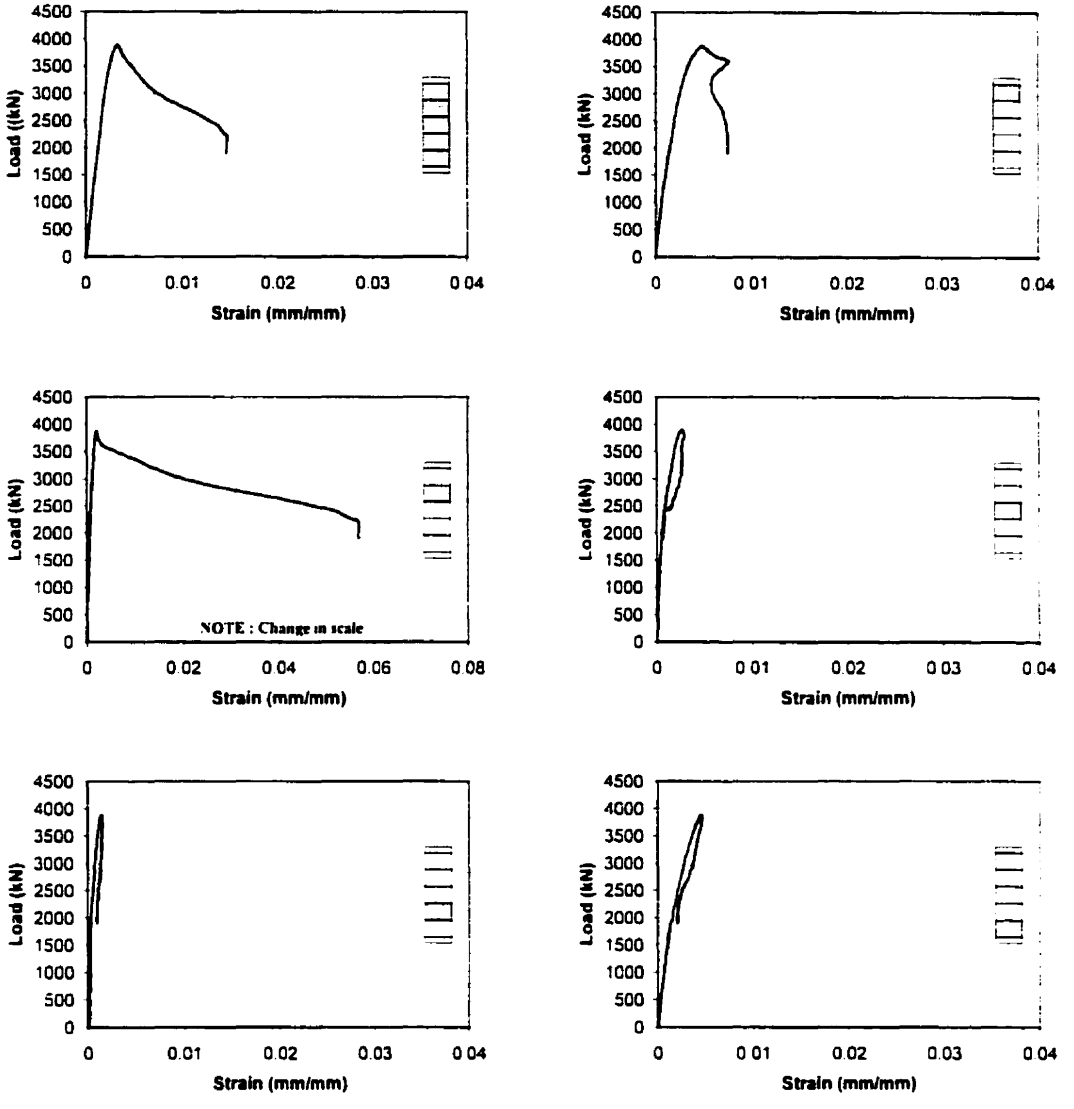

Figure 3.19: Load-strain responses of C40-400

3.5.2 Response of Specimen C40-500

The load-strain response for Specimen C40-500 is shown in Fig. 3.20. Unlike the previous specimen, Specimen C40-500 did not begin cracking near the top steel confining collar. Cracking began about one-third up the height of the column specimen. The cracking then quickly spread upwards until most of the specimen exhibited cracking. The spalling of the concrete cover began at a load of 3784 kN and an average longitudinal strain of 0.00324. Like Specimen C40-400, spalling is shown in Fig. 3.20 by a slight deviation in the slope of the load-strain response. The slope changed from a linear response to parabolic response. The confining effects of the spiral allowed this specimen's load carrying capacity to increase to a peak load of 3974 kN with an average longitudinal strain of 0.00451. From this point on, the load carrying capacity of this specimen dropped at a steep linear rate until the specimen failed. The specimen failed due to a rupture of the steel spiral resulting in the loss of confinement.

Since the spiral reinforcement ruptured in Specimen C40-500, the peak steel stress was approximately the ultimate stress of the steel (697 MPa). The strain gauges at mid-height gave different results. The first strain gauge yielded, while the second strain gauge reached about three-quarter of yield stress of the steel spiral. Therefore, the stress in the spiral had a significant strain variation. Figure 3.21 shows the load versus spiral strain response for Specimen C40-500.

Figure 3.22 shows the distribution of longitudinal strains over the five segments in Specimen C40-500. The strains in all five segments were similar until the crushing of the concrete. During the crushing of the concrete, the strain in segment two became many times greater than the strain in the other segments. The strain in the other four segments remained approximately constant.

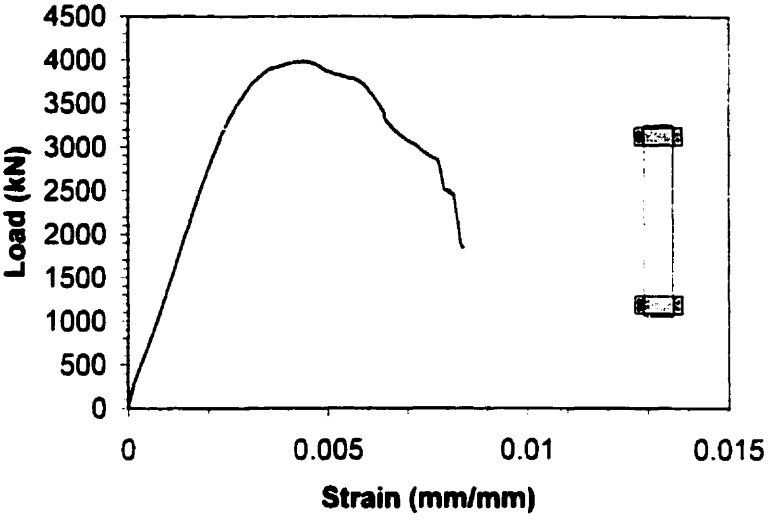

Figure 3.20: Average load-strain response for C40-500

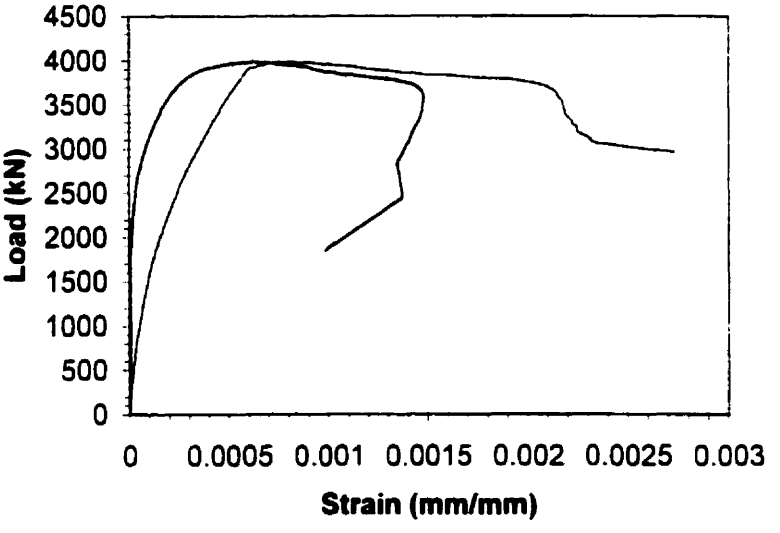

Figure 3.21: Spiral reinforcements strains for C40-500

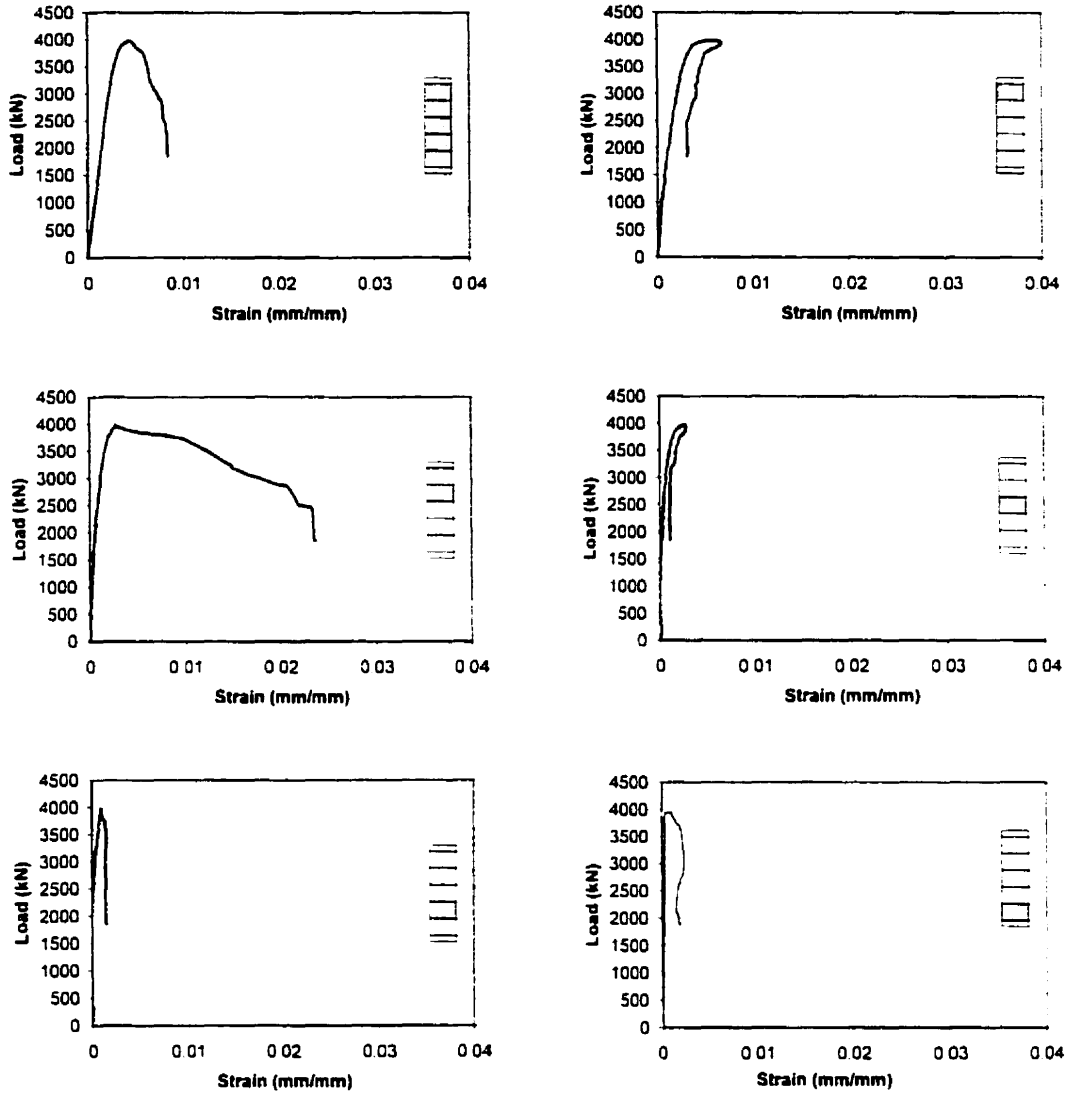

Figure 3.22: Load-strain responses of C40-500

3.5.3 Comparison of C40 Series

The peak loads of both reinforced C40 specimens differed by less than 2%. However, their strains at their peak loads were significantly different. Specimen C40-400's peak load occurred at a strain of 0.00323, while Specimen C40-500's peak load occurred at a strain of 0.00433. The rate of load decay after the peak load was also different. After its peak load was reached, Specimen C40-500's load dropped very steeply, while Specimen C40-400's load decayed in a more gradual manner. Figure 3.23 shows us the responses of the C40 specimens and Fig. 3.24 compares the C40 series after testing.

The energy absorbed or toughness of the specimens was significant for both specimens. The area under the load-strain curve being 41.43 kN for Specimen C40-400 and 24.68 kN for Specimen C40-500. The average longitudinal strain at the specimen's failure was 0.0145 for Specimen C40-400 and 0.0083 for Specimen C40-500.

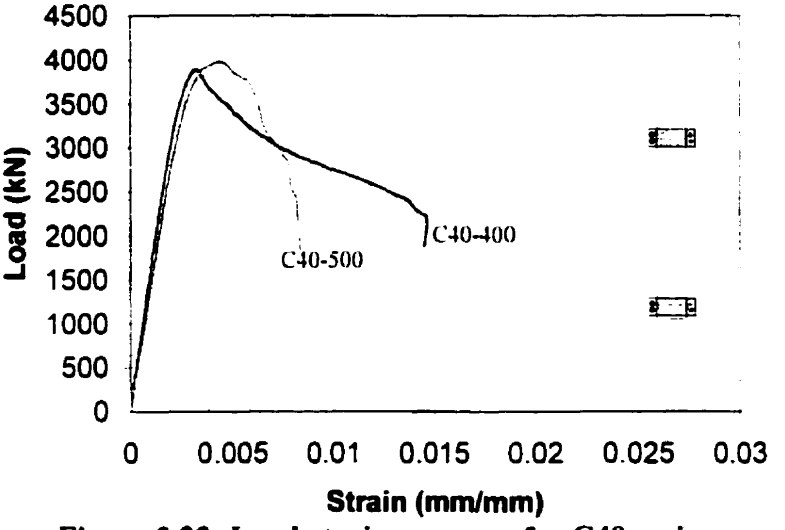

Figure 3.23: Load-strain response for C40 series

Figure 3.24: Photo of C40-400 and C40-500 at failure

3.6 Response of C60 series

The C60 series was instrumented with 8 LVDT's and 2 strain gauges as shown in Fig. 2.7 and Fig 2.9. The results are summarized in Table 3.2.

3.6.1 Response of Specimen C60-400

The load-strain response of Specimen C60-400 is shown in Fig. 3.25. At a load of 2250 kN, horizontal cracks developed at the mid-height of the specimen, much earlier than anticipated. However, these cracks did not seem to have any significant influence on the overall stiffness of the specimen. Specimen C60-400 reached a peak load of 3982 kN with an average longitudinal strain of 0.0038. Unlike the previous specimens, Specimen C60-400 did not exhibit a noticeable first peak or change in slope even after reaching an average longitudinal strain of approximately 0.0035, the typical concrete compressive strain limit. After the peak load was reached, the load carrying capacity of the specimen dropped, stabilizing at 3050 kN. Specimen C60-400 was able to sustain this load until the spiral ruptured at an average longitudinal strain of 0.0132. This initial spiral rupture caused the load carrying capacity of this specimen to drop by over 400 kN. The bond between the concrete and spiral was lost, causing the loss of confining stresses near the region of the rupture. After this initial rupture the vertical reinforcing bars began to buckle. The load continued to decay until the second rupture occurred. The second rupture in the spiral occurred at an average longitudinal strain of 0.0155. This caused the load to fall below half of the peak load and the test was stopped.

Figure 3.26 shows the load versus spiral strain response for specimen C60-400. Only one curve is shown on the graph because one strain gauge was damaged during casting and did not function. The second strain gauge was located near the region of initial cracking. Since the steel spiral ruptured it is evident that the spiral developed stresses greater than 653 MPa (ultimate stress), which indicates that a significant confinement effect was developed.

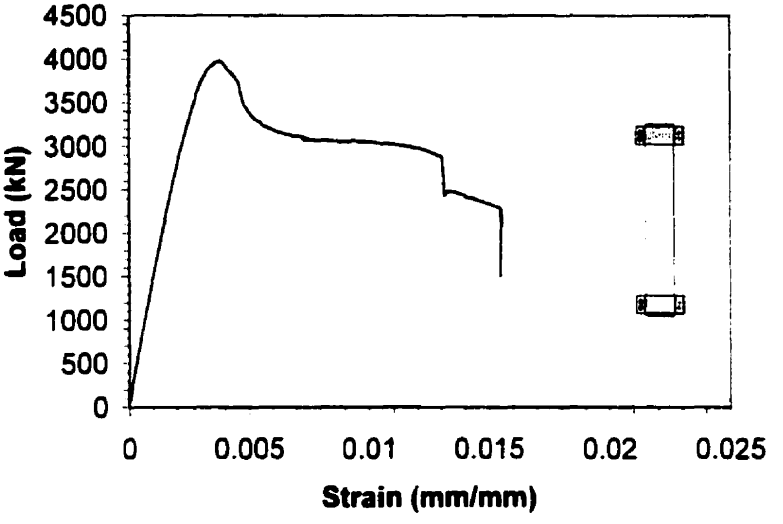

Figure 3.25: Average load-strain response for C60-400

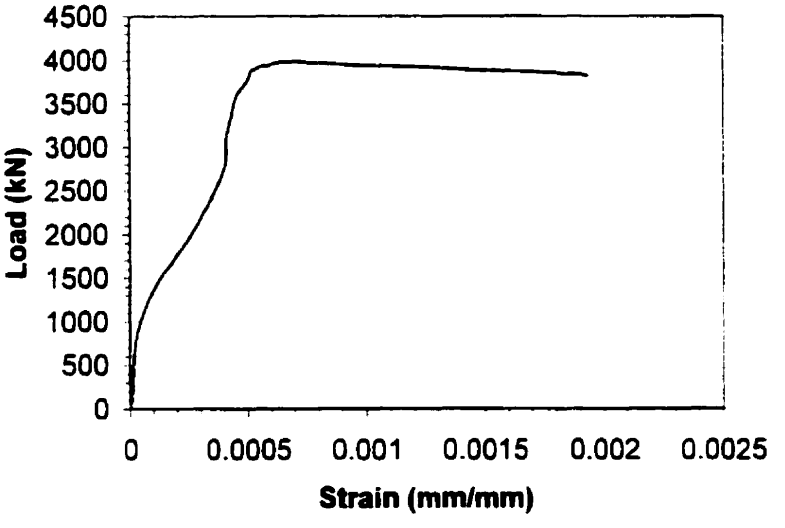

Figure 3.26: Spiral reinforcement strain for C60-400

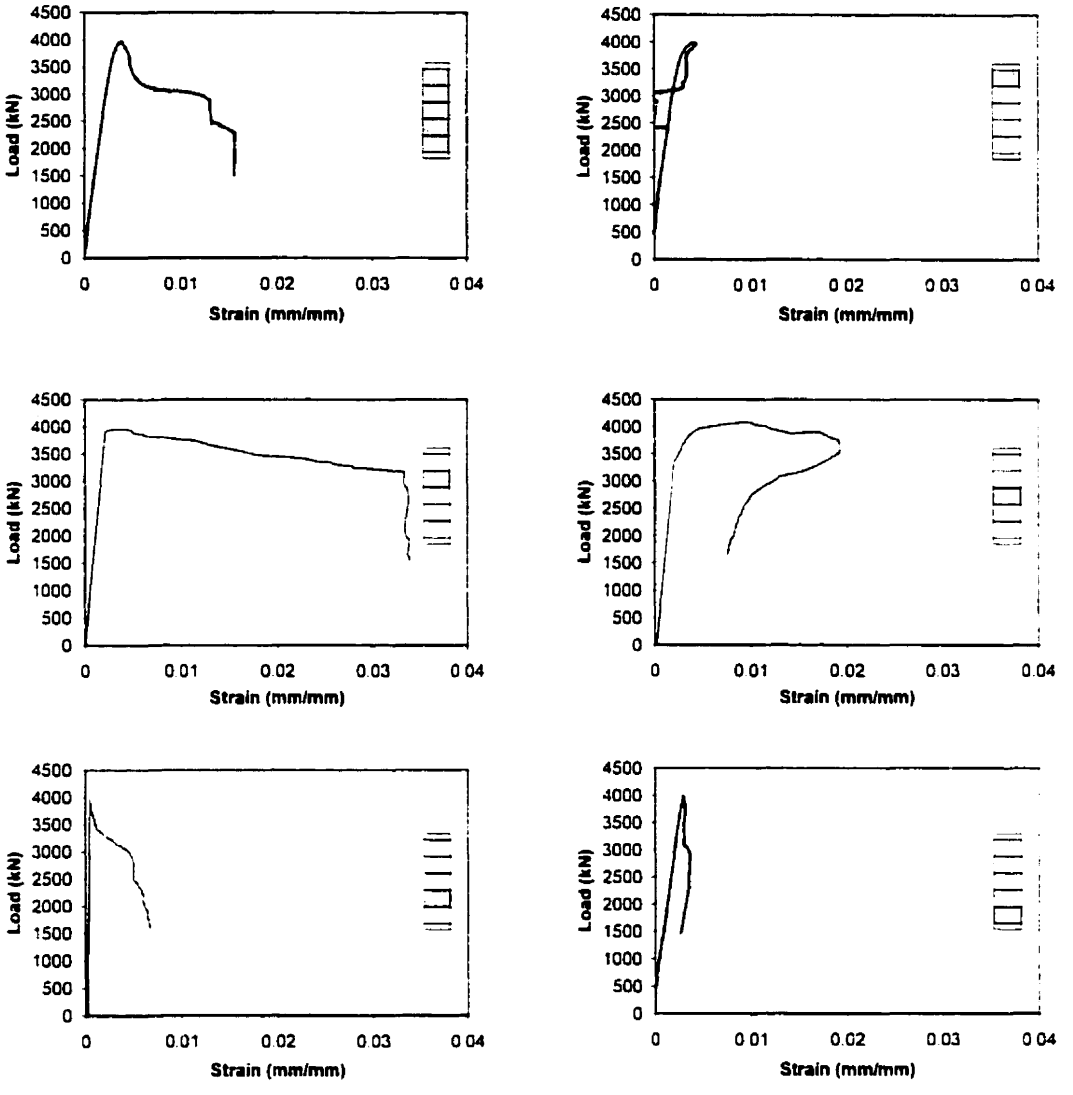

Figure 3.27: Load-strain responses of C60-400

All the concrete crushing and spiral rupturing occurred near in the mid-height of the specimen. Very little concrete crushing and no spiral ruptures were observed elsewhere. Figure 3.27 shows the strains in the five segments of the column. From these plots it is evident that the crushing was localized in two segments of the column.

3.6.2 Response of Specimen C60-500

The load-strain response of Specimen C60-500 is shown in Fig 3.28. Vertical cracking began near the top steel collar at a load of 3900 kN. A peak load of 4024 kN was reached at an average longitudinal strain of 0.00402. Like Specimen C60-400, it is difficult to notice any significant changes in stiffness due to the spalling. Spalling occurred progressively and only over the top third of the column. Once the peak load was reached, the load dropped rapidly, but stabilized at a constant decreasing rate until the spiral ruptured at an average longitudinal strain of 0.0676, causing the load carrying capacity of the specimen to decrease by 400 kN. After this first rupture, the load went back to its original load decay rate until a second rupture in the spiral occurred. A second rupture in the spiral occurred at an average longitudinal strain of 0.0786, causing the load carrying capacity of the specimen to fall by an additional 500 kN. Slight buckling of the vertical reinforcing bars was also observed after failure.

Both strain gauges on the spiral were relatively far from the location concrete. The spiral at the mid-height of the column reached only about one-quarter of its yield strain. However, stresses in the spiral were very much larger than the yielding stress at some locations since the spiral ruptured. Therefore, a wide variation in the spiral stress occurred in this specimen.

The load-strain responses for the five segments of Specimen C60-500 are shown in Fig 3.30. All of the crushing occurred over two segments.

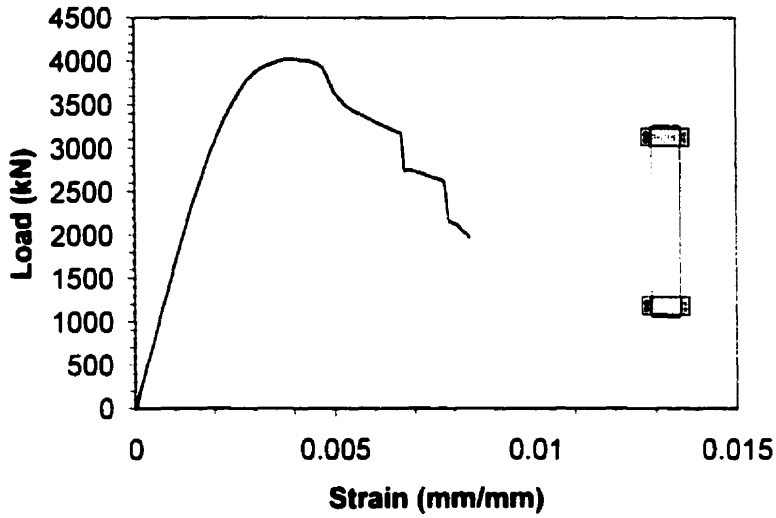

Figure 3.28: Average load vs strain response for C60-500

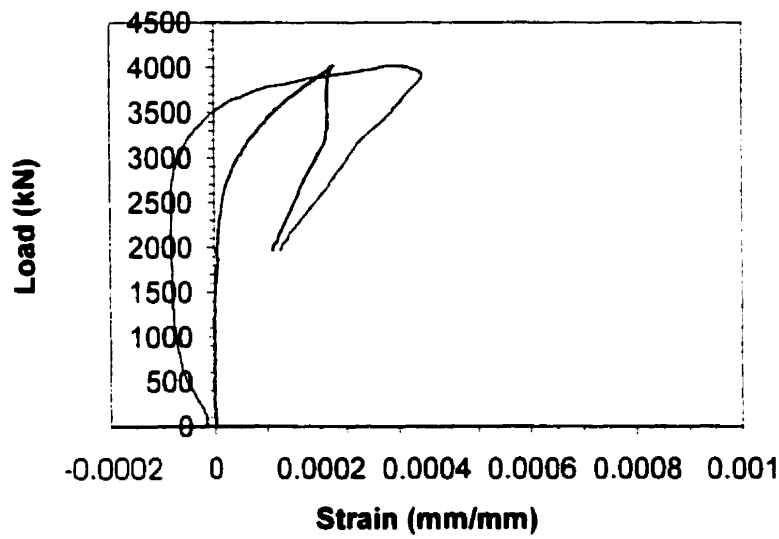

Figure 3.29: Spiral reinforcement strains for C60-500

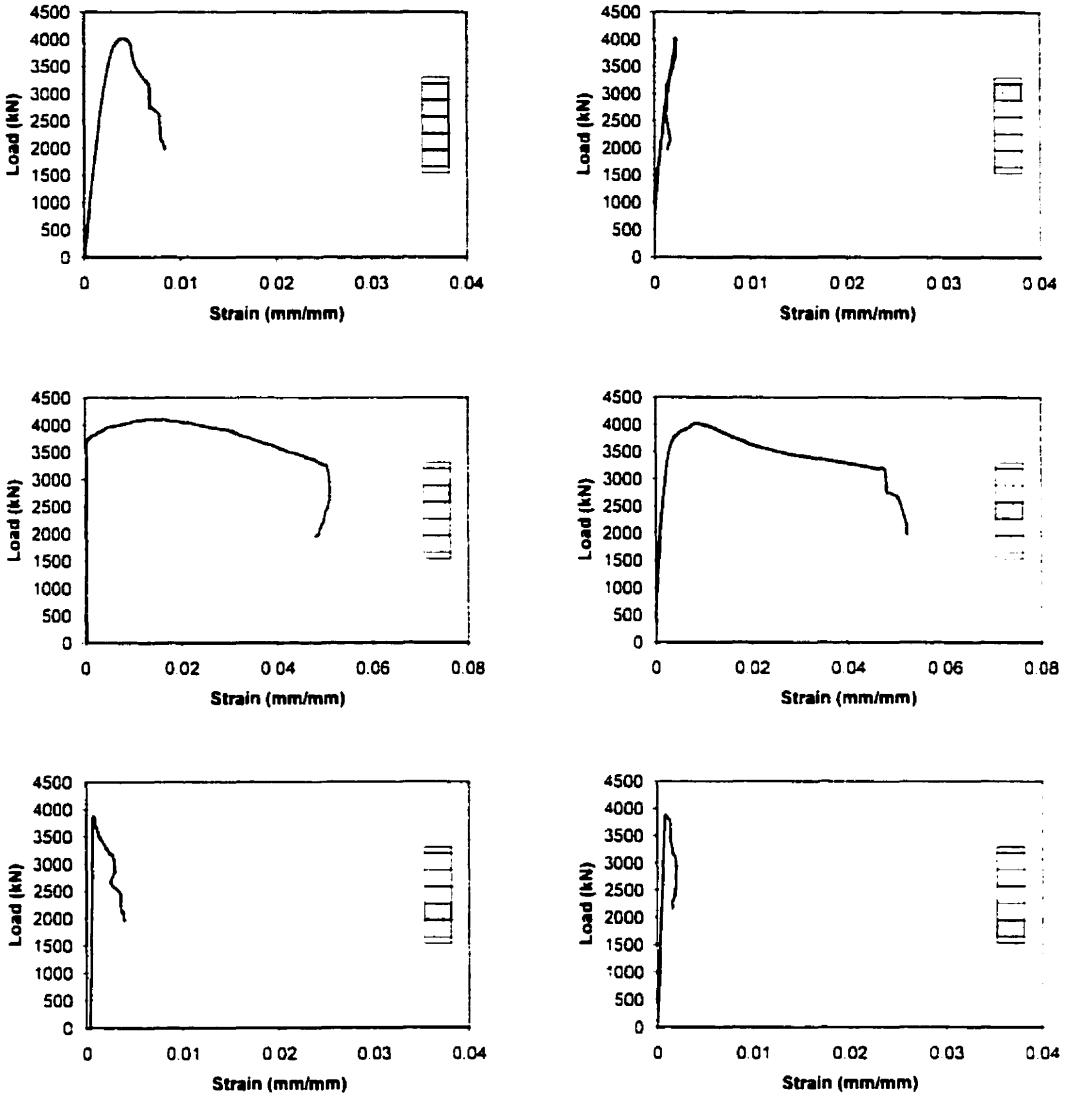

Figure 3.30: Load-strain responses of C60-500

3.6.3 Comparison of C60 Series

Figure 3.31 compares the response of both reinforced column specimens in the C60 series. Both C60 specimens have nearly identical load-strain responses, until the rupture of Specimen C60-500's spiral reinforcement. Their peak loads and their associated average strains at peak loads are also approximately equal. The failures of both specimens were very localized because the spalling of the concrete cover did not spread over the height of the specimen.

Specimen C60-400 displayed a greater toughness than Specimen C60-500. The area under the load-strain curve is 46.13 kN and 24.45 kN respectively, while the strain at $0.5f_{cc}$ on the descending branch is 0.0155 and 0.00823, for Specimens C60-400 and C60-500, respectively. Figure 3.32 shows a photograph of Specimens C60-400 and C60-500 following the test.

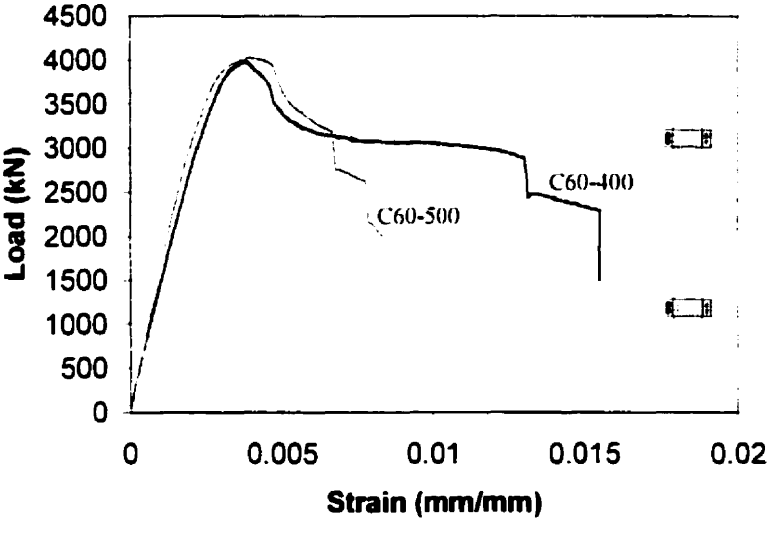

Figure 3.31: Load-strain response for C60 series

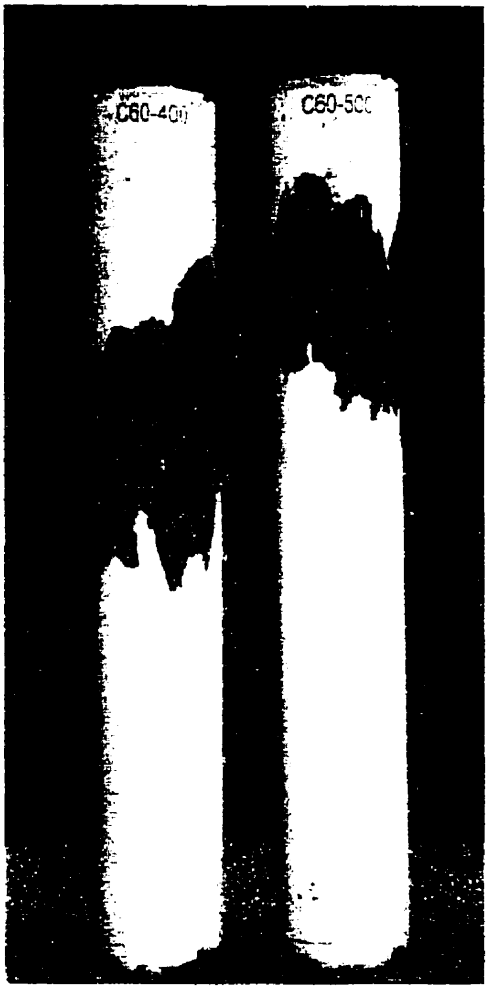

Figure 3.32: Photo of C60-400 and C60-500 at failure

3.7 Response of C100 series

The C100 series was instrumented with 4 LVDT's and 2 strain gauges as shown in Fig. 2.8 and Fig. 2.9. The results are summarized in Table 3.2.

3.7.1 Response of Specimen C100-400

The load-strain response of Specimen C100-400 is shown in Fig 3.33. Specimen C100-400 began to crack at its mid-height at a load of 5200 kN. The cracks quickly spread throughout the specimen as the loading increased. The load carrying capacity of Specimen C100-400 continued to increase linearly until a load of 5489 kN and at an average longitudinal strain of 0.00366 was reached. At this load the concrete cover spalled throughout the height of the column. The spalling of the concrete cover caused a slight drop in load. However, due to the confinement, the load carrying capacity of the specimen was able to increase after the concrete cover had spalled. Specimen C100-400 continued carrying additional load until the steel spiral yielded, with a peak load of 6222 kN and at an average strain of 0.00576. From this point on, the load decreased until it stabilized at a load of 4000 kN. The load stabilization was caused by the strain-hardening of the spiral steel. Specimen C100-400 continued to hold this load until the first rupture of the spiral reinforcement occurred at an average longitudinal strain of 0.0179. After this failure, the spiral began to rupture in several other locations. Buckling of the vertical reinforcing bars also contributed to the rupture of the spiral.

Figure 3.34 shows the load versus spiral strain response. One strain gauge was not functional. The functional strain gauge clearly shows that the strains in the spiral exceeded the yield strain. Stresses in the spiral steel were quite uniform because the concrete cover had spalled uniformly throughout the specimen.

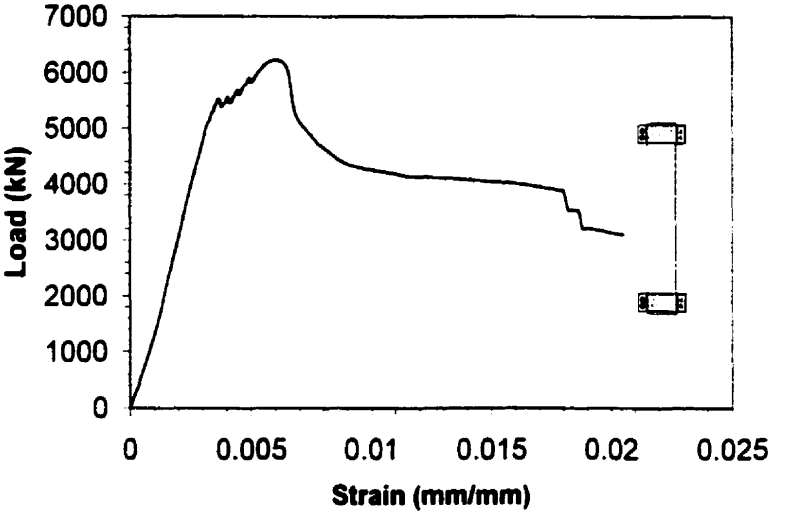

Figure 3.33: Average load-strain response for C100-400

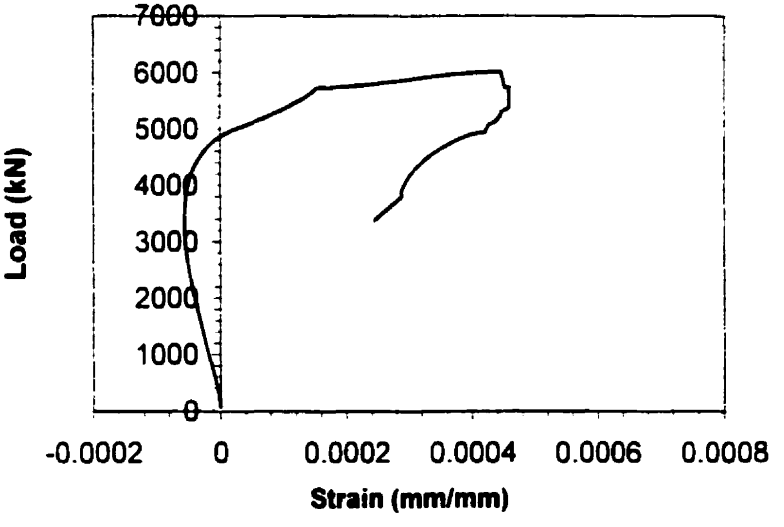

Figure 3.34: Spiral reinforcement strain for C100-400

3.7.2 Response of Specimen C100-500

Figure 3.35 shows the load-strain response for Specimen C100-500. Specimen C100-500 began to crack at a load of 5900 kN. In a manner similar to Specimen C100-400. these initial cracks spread throughout the test specimen. Upon reaching a compressive load of 6007 kN at an average longitudinal strain of 0.00374, the concrete cover began to spall. Spalling occurred throughout the specimen. The confinement from the steel spiral increased the load carrying capacity of this test specimen until a peak load of 6598 kN at an average longitudinal strain of 0.00498. After reaching the yield stress of the steel spiral, the load dropped until stabilizing at about 5200 kN. At an average longitudinal strain of 0.0783 the spiral ruptured. No longitudinal bar buckling was observed. Many more ruptures occurred in the spiral. All the ruptures were in the same segment, one above the other, as shown on Fig 3.37.

Figure 3.36 shows the load versus spiral strain response for Specimen C100-500. One strain gauge was not functional. The functional strain gauge shows the significant straining of the spiral. The stress in Specimen C100-500's spiral clearly reached the ultimate stress since the spiral ruptured throughout the specimen.

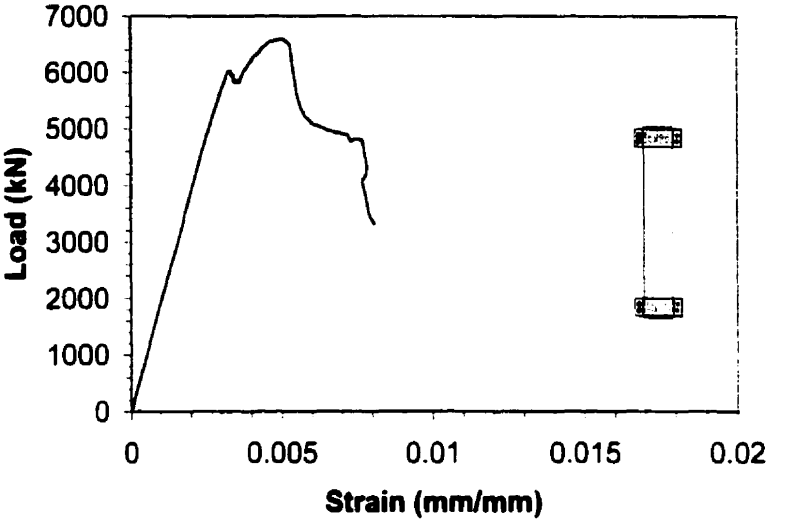

Figure 3.35: Average load-strain response for C100-500

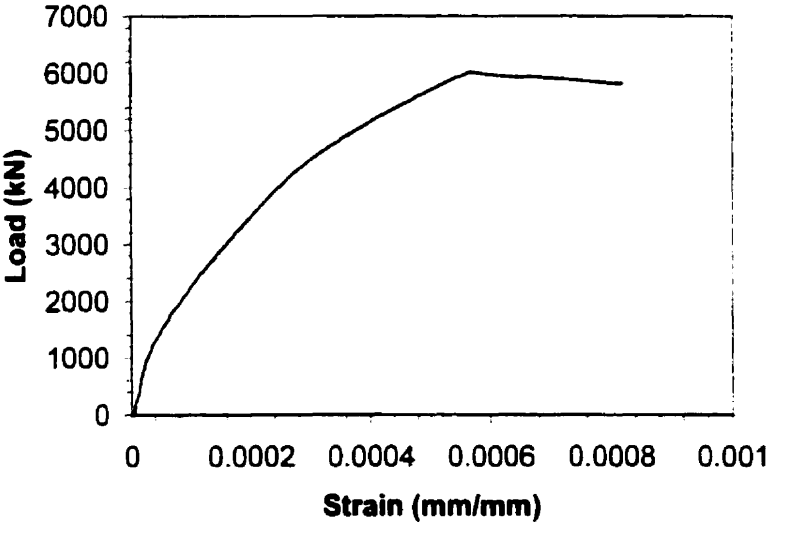

Figure 3.36: Spiral reinforcement strain for C100-500

Figure 3.37: Ruptures in steel spiral in Specimen C100-500

3.7.3 Comparison of C100 Series

Figure 3.38 compares the load-strain response of specimens C100-400 and C100-500. Both specimens exhibited similar responses until the initial rupture of the spiral reinforcement in Specimen C100-500. The peak loads differed by about 6%, but their strains at peak load were similar. The rate of load decay for both specimens is also similar.

The only significant difference between both specimens is in their toughness. Specimen C100-400 failed at an average longitudinal strain of 0.0206, while C100-500 failed at an average longitudinal strain of 0.0081, a ratio of about two to one. The ratio of areas under the load-strain curves also had a ratio of about two to one: Specimen C100-400 having a toughness of 84.13 kN, while Specimen C100-500 had a toughness of 42.19 kN.

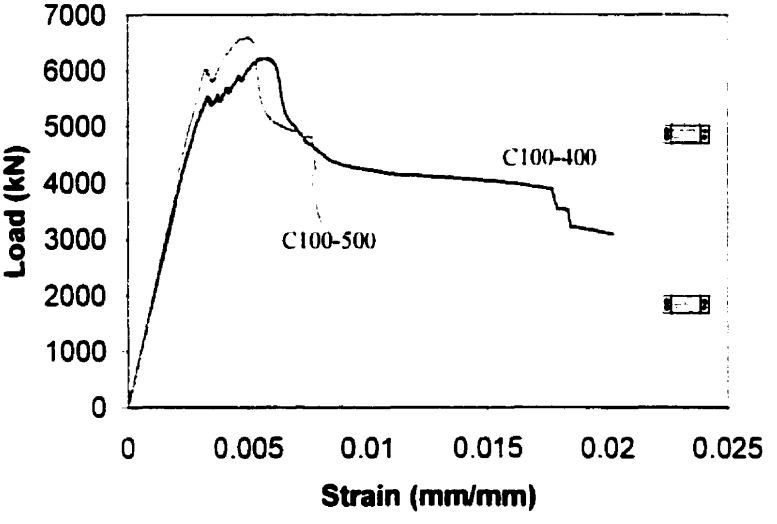

Figure 3.38: Load-strain response for C100 series

Figure 3.39: Photo of C100-400 and C100-500 at failure

3.8 Response of C120 series

The C120 series was instrumented with 4 LVDT's as shown in Fig. 2.8. Two strain gauges were included in each reinforced specimen, however they did not function. The results are summarized in Table 3.2.

3.8.1 Response of Specimen C120-400

Figure 3.40 shows the load-strain response for Specimen C120-400. The cracking of the concrete cover began near the top steel confining collar at a load of 5600 kN. This cracking continued until the concrete cover spalled at a load of 6427 kN with at an average longitudinal strain of 0.00551. A well-defined initial peak load was evident when the spalling of the concrete cover occurred. The spalling was extensive, occurring over the height of the specimen. After the spalling of the concrete cover, the load carrying capacity of Specimen C120-400 began to increase again, reaching a peak load of 7303 kN at an average longitudinal strain of 0.00905. This 876 kN increase in load carrying capacity was entirely attributed to the confinement provided by the steel spiral. Once the specimen's longitudinal strain reached 0.00939, the load carrying capacity of this specimen fell rapidly by over 1000 kN. After this sudden drop, the load stabilized and maintained a constant decay until the spiral ruptured. The first spiral ruptured at an average longitudinal strain of 0.00255. This initial rupture in the steel spiral was quickly followed by several other spiral ruptures throughout the specimen. Therefore, it can be concluded that the stress in the spiral must have been quite uniform. No strain gauge readings from the spiral were available because both strain gauges were not functional.

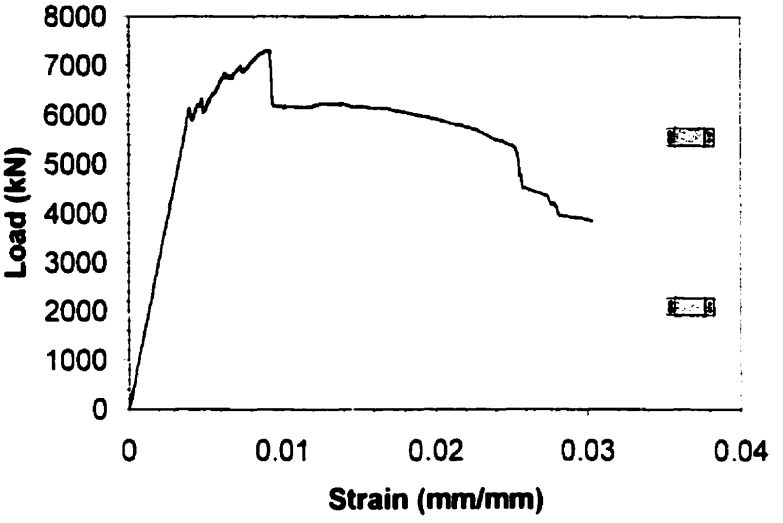

Figure 3.40: Average load-strain response for C120-400

3.8.2 Response of Specimen C120-500

Figure 3.41 shows the load-strain response for Specimen C120-500. Cracks in the concrete cover began to appear when a load of 7350 kN was reached. These initial cracks quickly spread throughout the specimen. When a load of 7387 kN was reached, at an average strain of 0.00554, the concrete cover spalled. This point is well defined on the load-strain response curve. The spalling of the cover caused a sudden drop in load, but due to the confining effects of the spiral, the specimen was able to increase its load carrying capacity to 7611 kN at an average longitudinal strain of 0.00756. After the peak load was reached, the load dropped 2000 kN. After this drop the load carrying capacity stabilized at 5800 kN. This load was maintained until the spiral ruptured. At a longitudinal strain of 0.0123, the spiral ruptured. No strain gauge readings from the spiral steel were available because both strain gauges were not functional.

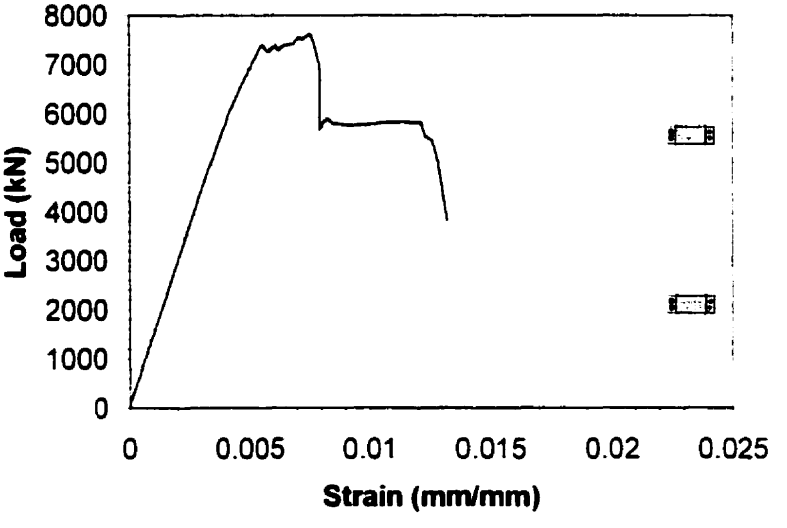

Figure 3.41: Average load-strain response for C120-500

3.8.3 Comparison of C120 Series

Figure 3.42 compares the load-strain responses of Specimens C120-400 and C120-500. The specimens behaved very similarly. Both specimens have well defined points where the spalling of the concrete cover occurred. Specimen C120-400 began spalling at a point of about 1000 kN before Specimen C120-500. However, both specimens attained approximately the same peak load (7303 kN compared with 7611 kN). The behaviour of the specimens following the yielding of the steel spirals was dramatic for both specimens. Specimen C120-500 reached its peak load at a lower longitudinal strain than Specimen C120-400. The strains at the peak loads for Specimens C120-400 and C120-500 were 0.00905 and 0.0756, respectively. See Fig. 3.43 for photographs of C120-400 and C120-500 at failure.

The toughness of both reinforced C120 specimens followed the same trend as the previous series, with Specimen C120-400 exhibiting more than twice the longitudinal strain at failure than for Specimen C120-500. The strains at failure were 0.00303 and 0.0132, for C120-400 and C120-500, respectively. The C120 series exhibited the largest toughness of all the series. The toughness of Specimen C120-400 is 102.99 kN compared with a 44.13 kN toughness for Specimen C120-500.

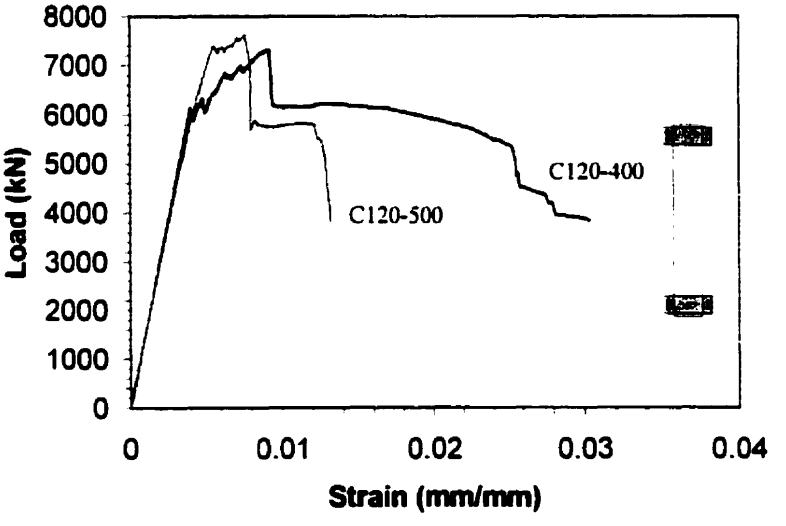

Figure 3.42: Load-strain response for C120 series

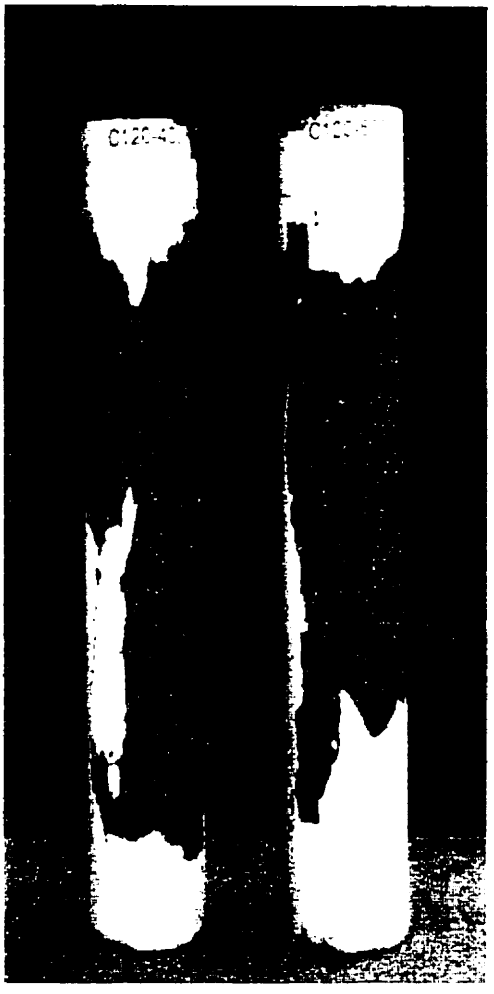

Figure 3.43: Photo of C120-400 and C120-500 at failure

Chapter 4

Analysis of Results

In this chapter, experimental results are compared to a prediction model based on the research of Cusson and Paultre (1995) and Mander, Priestley and Park (1988).

4.1 Prediction Model

The prediction model used in this experimental program requires few key variables. The important variables being the specified concrete compressive strength, f'_c, the yield stress of the transverse reinforcing steel, f_{yh}, the centre-to-centre spacing of the reinforcement, s, and the geometric properties of the specimen.

The unconfined concrete compressive strength, f'_c, enables the determination of the secant modulus, E_c and the value of the unconfined strain, ε_{co} from the following equations:

$$Ec = 3320\sqrt{f'_c} + 6900 \ MPa \tag{4.1}$$

$$\varepsilon_{co} = \frac{f'_c}{E_c}\frac{n}{n-1} \tag{4.2}$$

Where n, is a curve-fitting factor, given by the following equation:

$$n = 0.8 + \frac{f'_c}{17} \tag{4.2a}$$

4.1.1 Confinement Effects

The model used for the prediction of confined concrete response is based on the model proposed by Richart, Brandtzaaeg, Brown (1928). The following equation summarizes the Richart *et al.* model.

$$f_{cc} = f_{co} + 4.1 f_l \tag{4.3}$$

where,

f_{co} = maximum compressive strength of a plain concrete member,

f_{cc} = compressive strength of confined concrete,

f_l = lateral confining pressure applied on the concrete core from transverse reinforcement.

The unconfined concrete strength of a reinforced column is given as:

$$f_{co} = \alpha_1 f_c' \tag{4.4}$$

where,

α_1 = stress block factor is given as in the 1994 CSA A23.3 Standard:

$$\alpha_1 = 0.85 - 0.0015 f_c' \tag{4.4a}$$

The transverse confinement steel is assumed to have yielded at the peak load, therefore the confining stress in the concrete core, f_l, is given as:

$$f_l = \frac{2 A_{vp} f_{vh}}{d_c s} \tag{4.5}$$

The concrete confining stress, f_l is multiplied by a confinement effectiveness coefficient, k_e. The confinement effectiveness coefficient was developed by Mander, *et al.* (1988). It assumes that arching actions exist between the spirals and therefore the average confinement

stress is less than that predicted by statics. The effective lateral confinement stress is therefore given as:

$$f_{le} = k_e f_l \tag{4.6}$$

where,

k_e, the effective confinement coefficient is given as:

$$k_e = \frac{1 - \frac{s}{d_s}}{1 - \rho_g} \tag{4.7}$$

where,

d_s = diameter of spiral.

s = clear spacing between the spiral.

ρ_g = volumetric ratio of longitudinal reinforcement in the column cross-section.

4.1.2 Predicted Stress-Strain Curve

The prediction model is divided into two parts, the ascending and the descending branches as shown on Figure 4.1. The ascending branch (OA) of the specimen's stress-strain response is based on the work of Popovics (1973) and is given as:

$$f_c = f_{cc}\left[\frac{k\frac{\varepsilon_c}{\varepsilon_{cc}}}{k-1+\left(\frac{\varepsilon_c}{\varepsilon_{cc}}\right)^k}\right] \tag{4.8}$$

where, k, is a coefficient affecting the slope of the descending branch of the stress-strain curve, and is given as:

$$k = \frac{E_c}{E_c - \frac{f_{cc}}{\varepsilon_{cc}}} \tag{4.9}$$

where, ε_{cc}, the axial strain corresponding to maximum compressive strength of the confined concrete (based on the work of Cusson and Paultre (1995)) is given as:

$$\varepsilon_{cc} = \varepsilon_{co} + 0.21\left(\frac{f_{le}}{f_c'}\right)^{1.7} \tag{4.10}$$

The descending branch of the stress-strain response of a circular confined concrete column is based on the research of Fatitis and Shah (1985). They proposed the following stress-strain relation:

$$f_c = f_{cc} \cdot \exp\left[k_1(\varepsilon_c - \varepsilon_{cc})^{k_2}\right] \tag{4.11}$$

where k_1, the coefficient affecting the slope of the descending branch of the stress-strain response, is given as:

$$k_1 = \frac{\ln 0.5}{(\varepsilon_{c\,50c} - \varepsilon_{cc})^{k_2}} \tag{4.12}$$

where $\varepsilon_{c\,50c}$, the axial strain corresponding to $0.5f_{cc}$ is given as:

$$\varepsilon_{c\,50c} = 0.004 + 0.15\left(f_{le}/f_{co}\right)^{1.1} \tag{4.13}$$

and k_2, the coefficient affecting the curvature of the descending branch of the stress-strain response is given as:

$$k_2 = 0.58 + 16\left(f_{le}/f_{co}\right)^{1.4} \tag{4.14}$$

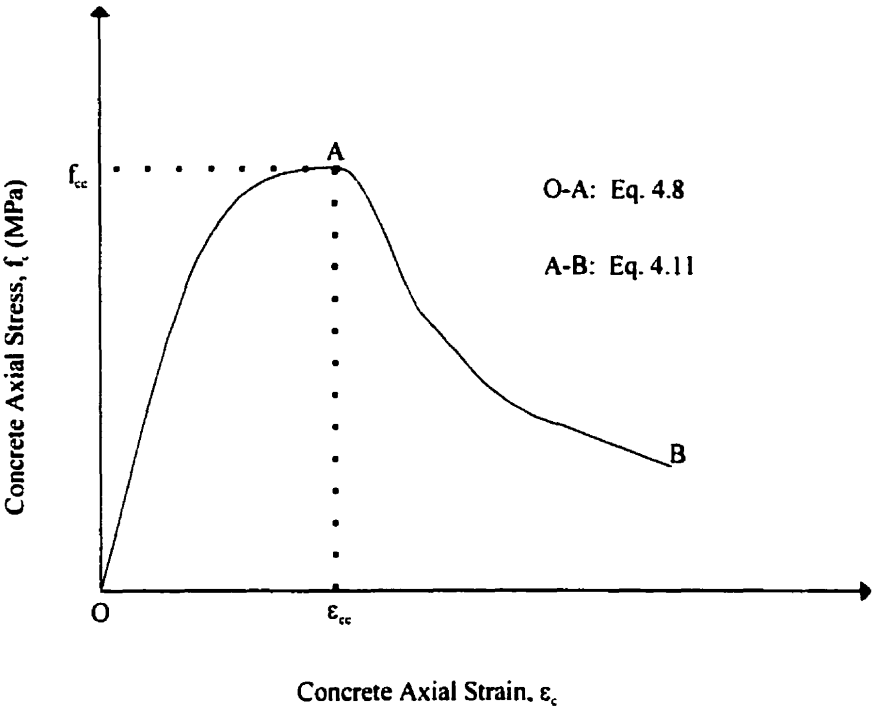

Figure 4.1: Predicted Stress-Strain Model

$$f_c = f_{cc}\left[\frac{k\frac{\varepsilon_c}{\varepsilon_{cc}}}{k-1+\left(\frac{\varepsilon_c}{\varepsilon_{cc}}\right)^k}\right] \tag{4.8}$$

$$f_c = f_{cc}\cdot\exp\left[k_1\left(\varepsilon_c-\varepsilon_{cc}\right)^{k_2}\right] \tag{4.11}$$

4.1.3 Predicted Load-Strain Response

The comparison between the predicted stress-strain response using the described model and the experimental results is difficult because of the presence of the longitudinal steel. To simplify the comparison, the prediction will be based on a load-strain response.

To convert the stress-strain prediction into a load-strain prediction, the concrete's compressive stress must be multiplied by the effectively stressed area. However, the concrete's effectively stressed area does not remain constant throughout the experiment. Initially, the entire concrete column cross-section ($A_g - A_s$) can be assumed to be stressed, but once a critical compressive strain in the concrete is reached, the concrete cover will spall. After this spalling, the concrete cover becomes ineffective, and hence only the concrete core, A_c, is effectively stressed.

To model this problem, it was assumed that the concrete cover will spall when, ε_{co}, the maximum compressive strain of unconfined concrete using Eq. 4.2 is reached. The concrete stress prior to this critical strain is assumed to be the unconfined stress on the full concrete cross-section (A_g-A_s). The concrete's stress following this critical strain, ε_{co}, is assumed to be the fully confined concrete stress on the concrete core, A_c.

The contribution of the longitudinal steel is also included in this model. The amount of load carried by the longitudinal bars is based on the strain in the longitudinal steel. To obtain the load carried by the longitudinal steel bars, the longitudinal strain of the steel is assumed to be equal to the longitudinal strain of the concrete. The steel's contribution increases linearly until the steel yields. Once the longitudinal steel has yielded, its load carrying contribution is assumed to remain constant.

Figure 4.2 shows the load-strain prediction model used. Equation 4.15 is used to predict the specimen's response until the concrete cover spalls at ε_{co}. Note that the unconfined concrete strength is used, and the full concrete cross-sectional area is in effect. Equation 4.16 is used to model the response between points A and B on Fig. 4.2. Note, that between points A and B the confined concrete stress is used and only the area of the concrete

core, A_c, is assumed to carry load. Equation 4.17 is used to model the response of the descending branch, points B to C on Fig. 4.2.

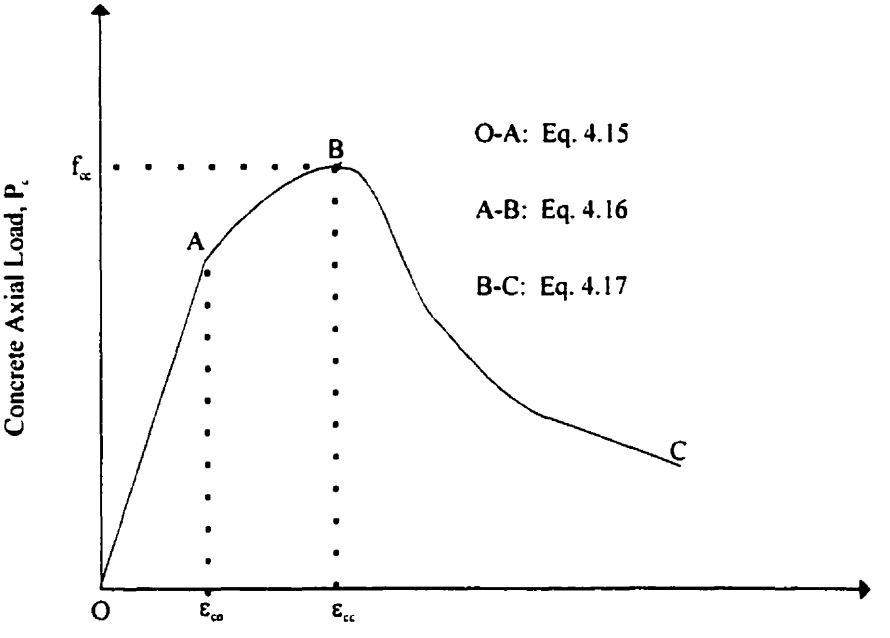

Figure 4.2: Load-Strain Prediction Model

$$P(\varepsilon_c) = f_{co}\left[\frac{k\frac{\varepsilon_c}{\varepsilon_{cc}}}{k-1+\left(\frac{\varepsilon_c}{\varepsilon_{cc}}\right)^k}\right](A_g - A_s) + A_s f_s \tag{4.15}$$

$$P(\varepsilon_c) = f_{cc}\left[\frac{k\frac{\varepsilon_c}{\varepsilon_{cc}}}{k-1+\left(\frac{\varepsilon_c}{\varepsilon_{cc}}\right)^k}\right](A_c) + A_s f_s \tag{4.16}$$

$$P(\varepsilon_c) = f_{cc} \cdot \exp\left[k_1(\varepsilon_c - \varepsilon_{cc})^{k_2}\right](A_c) + A_s f_s \tag{4.17}$$

4.2 Comparison with Experimental Results

The predicted load-strain responses versus the experimental results are presented on Fig. 4.3 through Fig. 4.7. The peak loads predicted are similar to the experimentally measured results. The predicted ductility closely mirrors the measured ductility of the experimental specimens and the descending branch of the load-strain curve is also similar. A noticeable difference that was exhibited in nine out of ten specimens, was that the predicted stiffness was slightly stiffer than that measured experimentally.

Table 4.1:Predicted Results versus Experimental Results

	Predicted		Experimental		% Difference	
	P_{max} (kN)	ε_{cc} (mm/mm)	P_{max} (kN)	ε_{cc} (mm/mm)	P_{max} (%)	ε_{cc} (%)
C30-400	3000	0.0060	2789	0.0049	7.6	22.4
C30-500	2936	0.0053	2771	0.0024	6.0	120.8
C40-400	3640	0.0043	3893	0.0033	-6.5	30.3
C40-500	3576	0.0040	3984	0.0044	-10.2	-9.1
C60-400	4237	0.0056	3982	0.0038	6.4	47.4
C60-500	4088	0.0047	4024	0.0039	1.6	20.5
C100-400	6958	0.0064	6222	0.0058	11.8	10.3
C100-500	6640	0.0054	6598	0.0050	0.6	8.0
C120-400	7489	0.0073	7303	0.0091	2.5	-19.8
C120-500	7208	0.0063	7611	0.0076	-5.3	-17.1

Table 4.1 compares the experimental results of the ten confined concrete columns with the predictions from the proposed model. The difference between the predicted peak load and experimental peak load was an average of 5.9%. The proposed model under-predicted the peak load in 8 out 10 specimens. The percentage difference varied from a low of 0.6% for Specimen C100-500 to a high of 11.8% for Specimen C100-400. The proposed model also has a smaller percentage difference in the predicted peak load for high-strength members than the normal-strength concrete specimens. The proposed prediction model had a more varied result for the strain prediction at the peak load. The percentage difference between the predicted model and experimental specimens varied from a low of 8 % to a high of 120.8%. The average percentage difference being 30.6%. The difference is high because of the difficulty in predicting post-peak behaviour. Specimen C30-500 has the largest

percentage difference between the experimental results and the predicted model. Figure 4.3 shows why the difference was so large. Specimen C30-500 showed significant ductility. After the peak load was reached, its load carrying capacity dropped slightly, but stayed relatively constant. But, there was no second peak. After the concrete had spalled, the additional load carrying capacity due to the confining forces were unable to make up the load carrying capacity lost due to spalling. The prediction model assumed a second peak in the stress-strain response, therefore there is a high percent difference in peak strain in specimens that did not have a second peak.

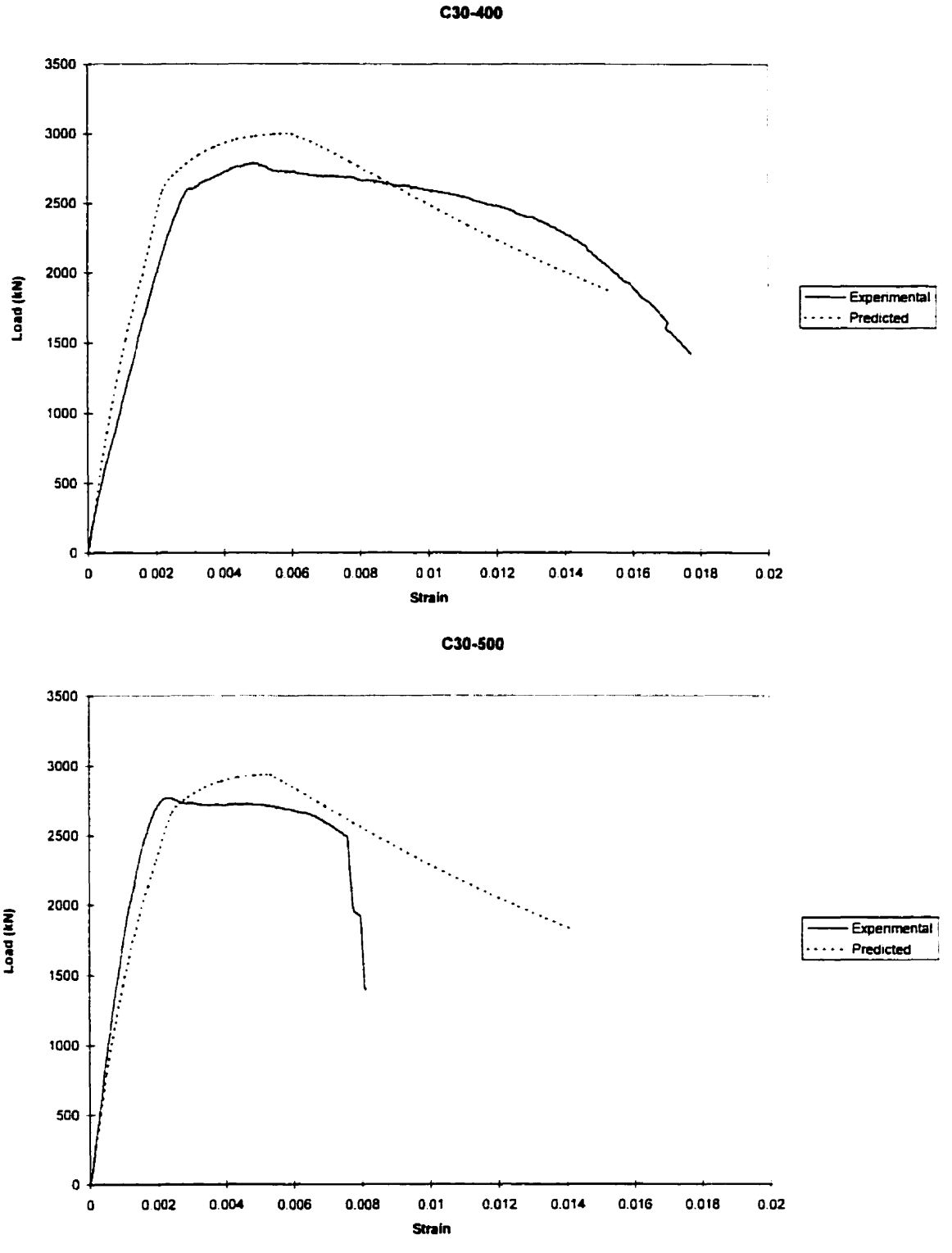

Figure 4.3: Predicted vs Experimental Results for C30 series

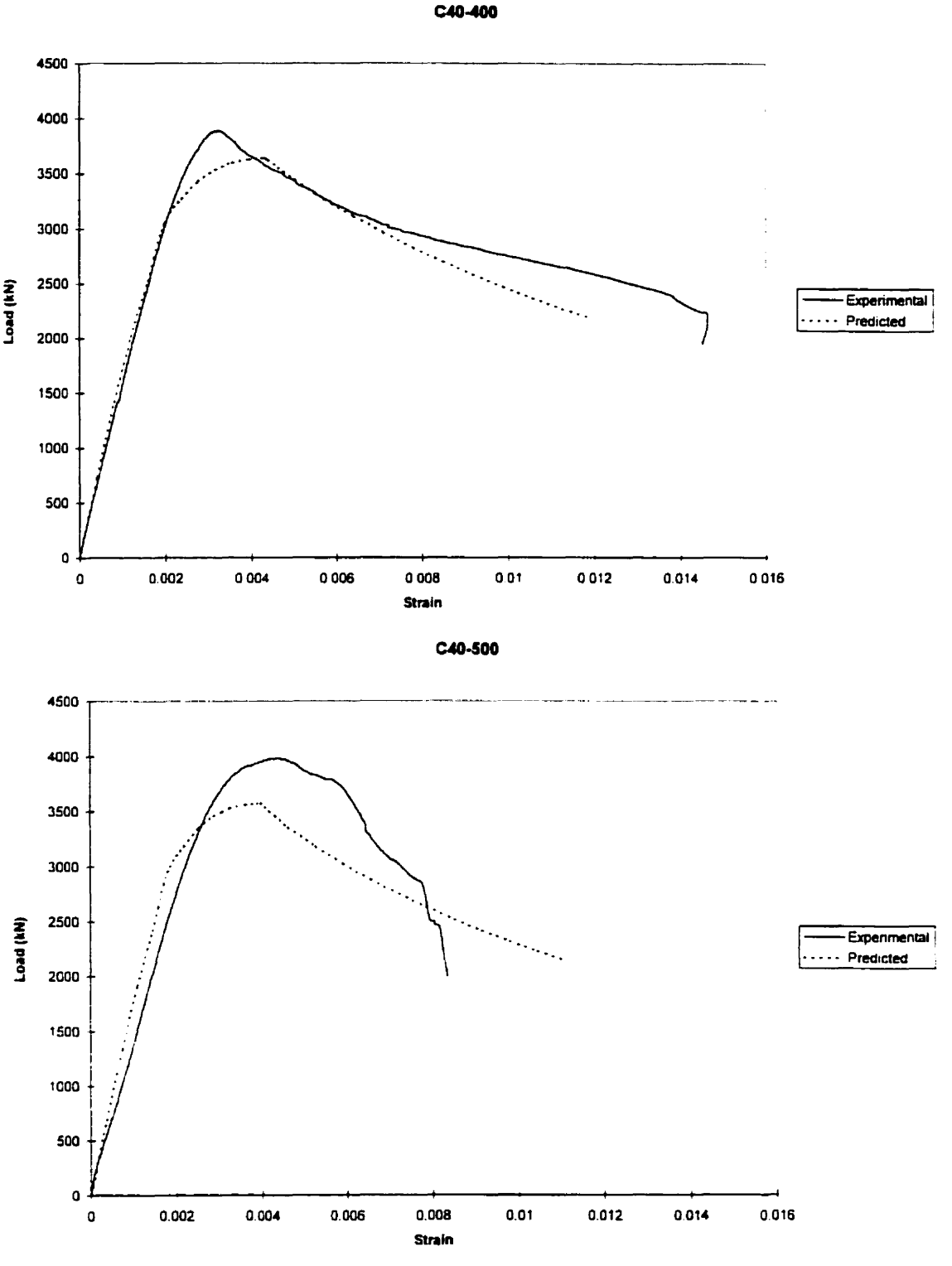

Figure 4.4: Predicted vs Experimental Results for C40 series

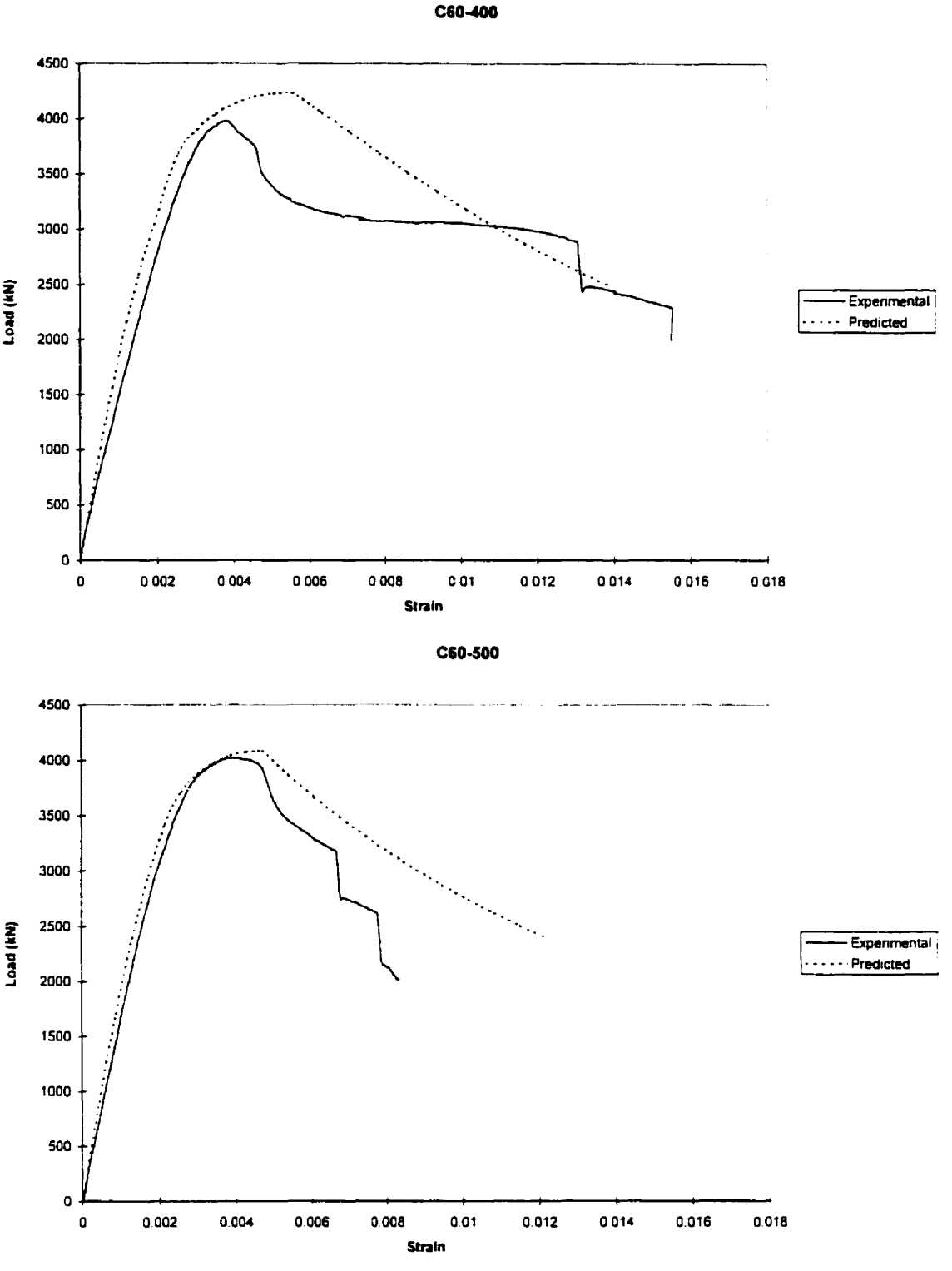

Figure 4.5: Predicted vs Experimental Results for C60 series

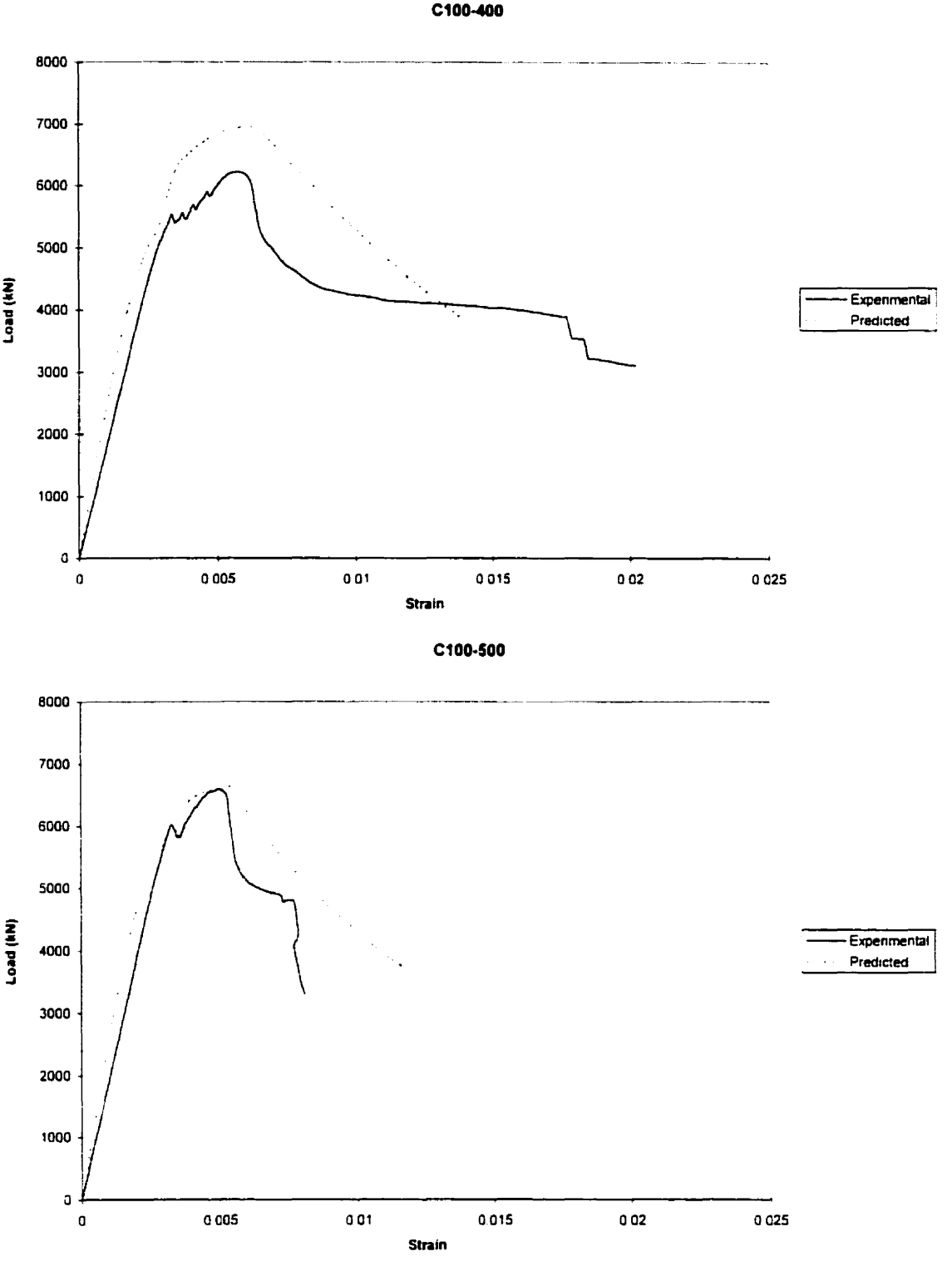

Figure 4.6: Predicted vs Experimental Results for C100 series

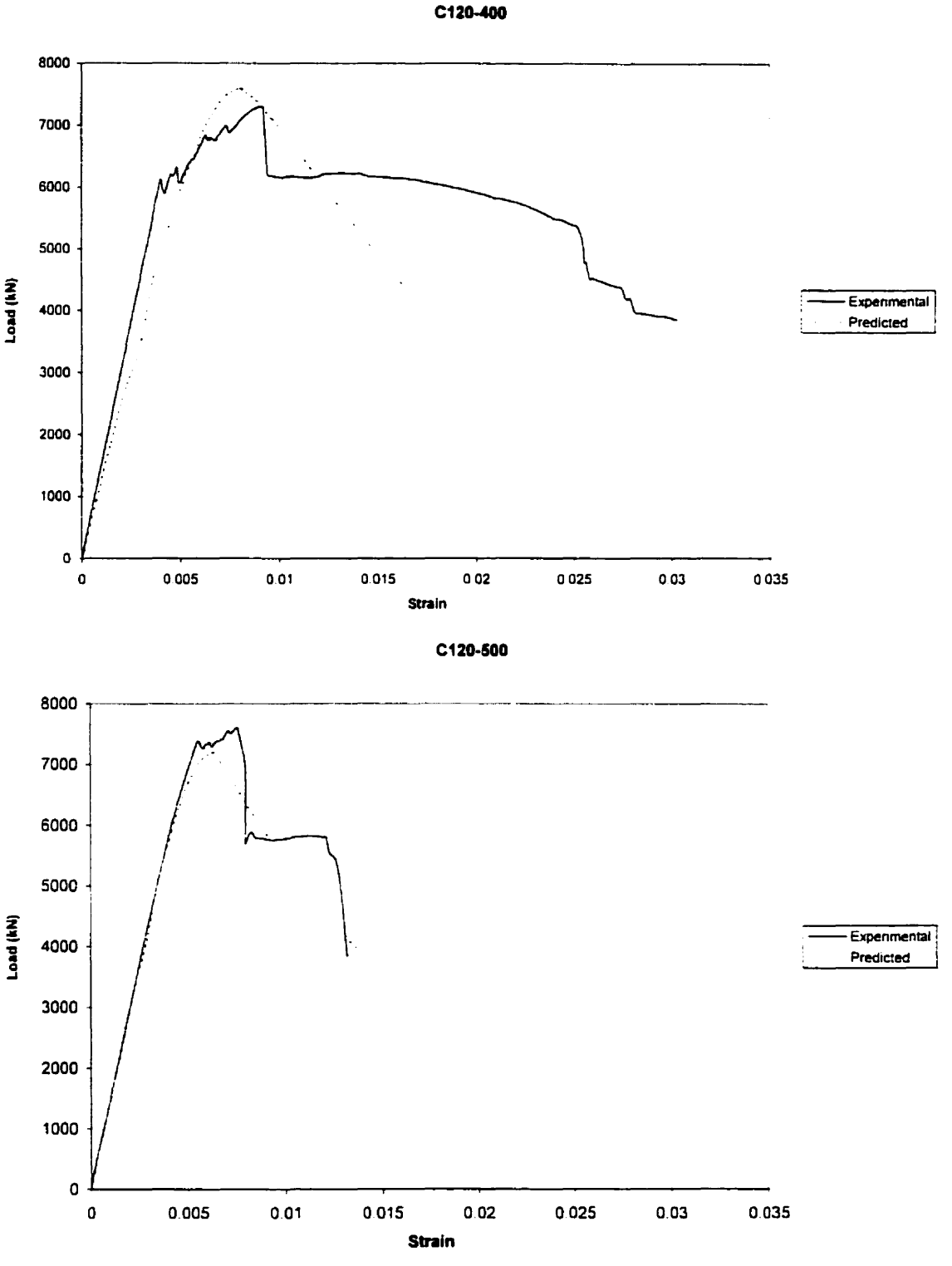

Figure 4.7: Predicted vs Experimental Results for C120 series

4.3 Comparison of Experimental Results to that Predicted using Code Equations

Table 4.2 compares the experimental results to those predicted by the ACI Code, CSA Standard and NZS Standard. The percentage difference varied significantly depending on the code used. The average percent difference for the ACI, CSA, and NZS codes are 12.80%, 7.24% and 7.81%, respectively.

Table 4.2: Experimental Results versus Predictions from Code Equations

	Experimental	ACI[1]	CSA[2]	NZS[3]	ACI	CSA	NZS
Specimen	P_{max} (kN)	P_o (kN)	P_o (kN)	P_o (kN)	% Difference	% Difference	% Difference
C30-400	2789	2883	2748	2883	3.37	-1.46	3.37
C30-500	2771	2883	2748	2883	4.04	-0.82	4.04
C40-400	3893	3337	3140	3337	-14.28	-19.35	-14.28
C40-500	3984	3337	3140	3337	-16.24	-21.20	-16.24
C60-400	3982	4343	3963	4265	9.06	-0.48	7.10
C60-500	4024	4343	3963	4265	7.92	-1.52	5.98
C100-400	6222	7995	6458	7141	28.50	3.80	14.77
C100-500	6598	7995	6458	7141	21.18	-2.11	8.23
C120-400	7303	8328	6647	7435	14.04	-8.98	1.80
C120-500	7611	8328	6647	7435	9.42	-12.66	-2.32

[1]ACI: $P_o = 0.85 f'_c A_c + F_y A_{st}$

[2]CSA: $P_o = \alpha_1 f'_c A_c + F_y A_{st}$: $\alpha_1 = 0.85 - 0.0015 f'_c$:but not less than 0.67

[3]NZS: $P_o = \alpha_1 f'_c A_c + F_y A_{st}$: $\alpha_1 = 0.85$: (for f'c less or equal to 55 MPa)
$\alpha_1 = 0.85 - 0.004(f'_c - 55)$ but not less than 0.75: (for f'_c greater than 55 MPa)

The CSA Standard gave the best predictions and was the most conservative code with nine out of ten predictions being less than the experimental results. The NZS Standard also gave good predictions, but over-predicted the peak strength in 7 out of 10 specimens. The ACI approach was the least conservative approach and had the highest percent difference between the predicted and experimental value. Clearly the CSA and NZS Standard approaches of reducing the stress block factor, α_1, with increasing concrete strength is a better approach.

4.4 Predicted Response for Plain Concrete Specimens

The plain concrete specimens were predicted using the specified concrete strength, f'_c. Predictions were made using the ACI Code, CSA Standard, and NZS Standard. The following equation was used to predict the plain concrete column's peak compressive stress:

$$P = \alpha_1 f'_c A_c \tag{4.18}$$

where,

ACI: $\alpha_1 = 0.85$

CSA: $\alpha_1 = 0.85 - 0.0015 f'_c$

NZS: $\alpha_1 = 0.85$: (for $f'_c < 55$ MPa)

$\alpha_1 = 0.85 - 0.004(f'_c - 55)$: (for $f'_c \geq 55$, but not less than 0.75)

Table 4.3 presents the predictions for the plain concrete specimens using the ACI Code, CSA Standard and NZS Standard.

Table 4.3: Experimental Results versus Predictions for Plain Concrete Specimens

Specimen	Experimental	Predicted			% Difference		
	P_{max} (kN)	$P_{max(ACI)}$ (kN)	$P_{max(CSA)}$ (kN)	$P_{max(NZS)}$ (kN)	ACI (%)	CSA (%)	NZS (%)
C30-0	2368	2205	2067	2205	-6.9	-12.7	-6.9
C40-0	2861	2453	2282	2453	-14.3	-20.2	-14.3
C60-0	3278	3701	3312	3614	12.9	1.0	10.3
C100-0	5414	7446	5871	6570	37.5	8.4	21.4
C120-0	6859	7788	6064	6871	13.5	-11.6	0.2

The NZS Standard gave the best peak strength prediction for the plain concrete specimens. The average percent difference for the NZS Standard was 2.1% while average percent difference for the CSA Standard and ACI Code were –7% and 8% respectively. However, for very high-strength concrete the CSA Standard gave the best prediction. The CSA Standard is conservative for normal strength concrete, while the ACI Code and NZS Standard may not be conservative enough for high-strength concrete.

Chapter 5

Conclusions and Recommendations

The following conclusions were drawn from the results of the experimental program on the 15 column specimens

1) High-strength concrete can be made to perform adequately with proper confinement.
2) The confinement equations provided by our current codes provide sufficient lateral steel for confinement.
3) The use of high-strength steel for confinement of concrete is an effective way of reducing lateral steel reinforcement congestion in high-strength concrete columns.
4) The stress-strain model confined concrete proposed by Cusson and Paultre (1995) closely mirrored the actual experimental stress-strain response. The prediction model worked well for both high and normal-strength concrete.
5) The CSA Standard (CSA, 1994) design approach to designing high-strength concrete columns is most accurate. The ACI Code (ACI, 1989) and NZS Standard (NZS, 1995) design approaches may not be conservative for high-strength concrete columns.

It is hoped that the results obtained from this experimental program will help other research efforts in better understanding the mechanisms of the axial stress-strain response of confined concrete columns. It is hoped as well that the experimental data obtained will be of use to future researchers working towards improving current models for the axial stress-strain responses of confined concrete.

References

ACI Committee 105 (1933), *"Reinforced Concrete Column Investigation"*. ACI Journal, v4, pp. 275-282.

ACI Committee 318 (1989), *"Building Code Requirements for Structural Concrete (ACI 318-89) and Commentary (ACI 318RM-89)"*. American Concrete Institute, Detroit, 351 pp.

Ahmad, S.H., and Shah, S.P. (1982), *"Stress-Strain Curves of Concrete Confined by Spiral Reinforcement"*. ACI Journal, v79 No. 6, pp. 484-490.

Collins, M.P., Mitchell, D.(1997), *"Prestressed Concrete Structures"*. Response Publications, Canada. 766 pp.

Considère, A. (1903), "Resistance a la Compression du Beton Armé et du Beton Frette ". Genie Civil.

Cusson, D., and Paultre, P. (1993), *"Confinement Model for High-Strength Concrete Tied Columns"*. Rep. No.SMS-9302. Dept. of Civil Eng., University of Sherbrooke, Sherbrooke, Quebec, Canada.

Cusson, D., and Paultre, P. (1994), "High-*Strength Concrete Columns Confined by Rectangular Ties* ". J. of Struct. Engineering, ASCE, v120 No.3.

Cusson, D., and Paultre, P. (1995), *"Stress-Strain Model for Confined High-Strength Concrete* ". J. of Struct. Engineering, ASCE, v121 No.3, pp.468-477.

CSA Committee A23.3 (1994), *"Design of Concrete Structures with Explanatory Notes"*. Canadian Standards Association, Rexdale.

Fafitis, A., and Shah, S.P. (1985), *"Lateral Reinforcement for High-Strength Concrete Columns"*. ACI Spec. Publ. SP 87-12, ACI, pp213-232.

Iyengar, K.T.S.R., Desayi, P., Reddy, T.S. (1978), *"Equation for Stress-Strain Curve of Concrete Confined by Circular Steel Spirals* ". Materials and Structures, Research and Testing, v11 No.65.

Mander, J.B., Priestley, P., M.J.N., and Park, R. (1988),*"Theoretical Stress-Strain Model for Confined Concrete* ". J. of Struct. Engineering, ASCE, v114 No.8, pp.1804-1826.

Mander, J.B., Priestley, P., M.J.N., and Park, R. (1988), "Observed *Stress-Strain Behaviour for Confined Concrete* ". J. of Struct. Engineering, ASCE, v114 No.8, pp.1827-1849.

Martinez, S., Nilson, A.H., and Slate, F.P. (1984), *"Spirally Reinforced High-Strength Concrete Columns"*. ACI Journal, v81 No. 5, pp. 431-442.

NZS 3101 (1995), "*Code of Practice for the Design of Concrete Structures*". Standards Association of New Zealand, Wellington, New Zealand.

Pessiki, S., and Pieroni, A. (1997), "*Axial Load Behavior of Large-Scale Spirally-Reinforced High-Strength Concrete Columns*". ACI Journal, v94 No. 3, pp. 304-314.

Popovic. S. (1973), "*A Numerical Approach to the Complete Stress-Strain Curve of Concrete*". Cement and Concrete Res., v3 No.5, pp. 583-899.

Richart, F.E., Brandtzaeg, A., and Brown, R.L. (1928), "*A Study of the Failure of Concrete under Combined Compressive Stresses*". University of Illinois Engineering Experimental Bulletin No. 185. Urbana.

Richart, F.E., Brandtzaeg, A., and Brown, R.L. (1929), "*The Failure of Plain and Spirally Reinforced Concrete in Compression*". University of Illinois Engineering Experimental Bulletin No. 190, Urbana.

William, K.J, and Warnke, E.P. (1975), "*Constitutive Model for the Triaxial Behavior of Concrete*". Proc., International Association for bridge and Structural Engineering, v19, pp. 1-30.

Zahn, F.A., Park, R. and Priestley, M.J.N. (1987), "*The Use of Grade 380 Steel for Transverse Confining Reinforcement in Columns*". Bulletin of the New Zealand National Society for Earthquake Engineering, v20 No.2, pp 99-113.